福井大学リポジトリ
UNIVERSITY OF FUKUI
REPOSITORY

Reaction between Carbon Dioxide and Elementary Fluorine

メタデータ	言語: English 出版者: 公開日: 2008-03-26 キーワード (Ja): キーワード (En): 作成者: HASEGAWA, Yasuo, 長谷川, 安男 メールアドレス: 所属:
URL	http://hdl.handle.net/10098/1665

A Dissertation Submitted to the
University of Fukui for the Degree of
Doctor of Engineering

Reaction between Carbon Dioxide and Elementary Fluorine

March 2008

Yasuo Hasegawa

To
my family

Reaction between Carbon Dioxide and Elementary Fluorine March 2008 Yasuo Hasegawa

Preface

The study presented here has been carried out as the Doctor dissertation under the direction of Professor Dr. Masayuki Takashima, Center for Cooperative Research, University of Fukui, and Associate Professor Dr. Susumu Yonezawa, Department of Materials Science and Engineering, University of Fukui. The purpose of this work is to investigate the reaction between carbon dioxide and elementary fluorine. The author wishes that this study would lead to further development of technology for human life.

First, I would like to express my appreciation to Professor Dr. Masayuki Takashima for giving me the opportunity to take part in this exciting research project and offering me his suggestions, support, and patience throughout the process. Also, I would like to thank Associate Professor Dr. Susumu Yonezawa for his direction, advice, comments and helpful support throughout this work. This successful completion owes much to the support of them.

I could meet Professor Dr. Yoshio Yamada during my study. I also thank you for your friendship and guidance.

I am greatly indebted to the entire crew at the Inorganic Material Chemistry Laboratory of University of Fukui and the Forensic Science Laboratory of Fukui Prefectural Police Headquarters who helped and encouraged this work in various ways. My sincere gratitude is given to many peoples and I am thankful to my young colleagues and past members at Takashima Lab, Mr. Hiroyasu Otsuka, Mr. Satoshi Ueda, Mr. Takashi Yagi, Miss Reiko Otani, Mr. Akitomo Nagasaka, Mr. Hidezi Fukaya, Mr.

Shigeyuki Kimura, Dr. Shiori Nishibu and Dr. Jae–Ho Kim for their cooperation and support. Also, I wish to show my gratitude for the warm encouragement and support of my office members, Mr. Shigeki Matsumura, Mr. Tetsuya Tsukahara and Mr. Fukuzo Masuyama.

We gratefully acknowledge that the GC / FT–IR spectra were acquired for us by Mr. Mamoru Komatsu of Thermo Nicolet Japan Inc.

Once again, the success of this dissertation will owe a great deal to the peoples and groups mentioned above and I am very grateful to them for their contributions.

Table of contents

Preface

List of Figures vi

List of Tables x i

General Introduction 1

1 Global warming 1

2 Reaction between CO_2 and F_2 2

3 Objective of this study 5

References and notes 6

Chapter 1. Reaction between carbon dioxide and elementary fluorine 9

1.1 Introduction 9

1.1.1 Properties of fluorine 10

1.1.2 New energy cycle with CO_2 fixing process 13

1.2 Experimental 14

1.3 Results and Discussion 18

1.3.1 Reaction product 18

1.3.2 In the presence of metal fluorides 24

1.3.3 Yields 31

1.3.4 Reaction rate 36

1.3.5 Activation energy of COF_2 formation 37

1.3.6 Reaction mechanism 37

References and notes 43

Chapter 2. Preparation of COF_2 using CO_2 and F_2 in the electrochemical cell with $PbSnF_4$ as a solid electrolyte 46

2.1 Introduction 46

2.1.1 What is a CO_2 / F_2 electrochemical cell? 47

2.1.2 Electrochemical impedance spectroscopy 48

2.2 Experimental 53

2.2.1 Preparation of $PbSnF_4$ 53

2.2.2 Characterization of $PbSnF_4$ 54

2.2.3 Preparation of COF_2 56

2.3 Results and Discussion 58

2.3.1 Preparation of $PbSnF_4$ 58

2.3.2 Electrochemical properties 63

2.3.3 Preparation of COF_2 in an electrochemical cell 67

References and notes 70

Chapter 3. Conclusion and future work 73

3.1 Conclusion 73

3.1.1 Chapter 1 73

3.1.2 Chapter 2 74

3.2 Future work 75

List of publications 76

Articles of other works 78

List of Figures

Fig. 1.1. Apparatus for the reaction between CO_2 and F_2. (a) Gas–gas reaction line, (b) trap–to–trap separation line and (c) vacuum line. (1) CO_2 gas storage, (2) F_2 gas storage, (3) reactor (SUS316L), (4) constant volume container, (5) reactor pressure gauge, (6) CO_2 gas pressure gauge, (7) F_2 gas pressure gauge, (8) PIRANI gauge, (9) Ar or He gas cylinder, (10) gas sampler, (11) activated alumina, (12) trap (liq. N_2), and (13) vacuum pump (oil rotary) 15

Fig. 1.2. Calibration lines of CO_2 (a), COF_2 (b), CF_3OF (c) and CF_4 (d). (b)–1 and (b)–2 correspond, respectively, to data at 1930 cm^{-1} in Ref. [17] and Ref. [18]. (c)–1, (c)–2 and (c)–3 correspond to data at 1282 cm^{-1} in Ref. [19], at 1282 and at 945 cm^{-1} measured in this study 18

Fig. 1.3. Transient of the pressure change in the direct reactions at (a) 373 K, (b) 423 K, (c) 473 K, (d) 498 K and (e) 523 K. CO_2 : F_2 = 50.7 kPa : 101.3 kPa and reaction time 50 h 19

Fig. 1.4. FT–IR spectrum of the product in the direct reaction. CO_2 : F_2 = 76 kPa : 76 kPa, reaction temp. 498 K, and reaction time 24 h 20

Fig. 1.5. Gram–Schmide spectra of the product measured using GC / FT–IR. CO_2 : F_2 = 50.7 kPa : 101.3 kPa, reaction temp. 498 K, and reaction time 50 h 20

Fig. 1.6. GC / FT–IR spectra of the products at retention times of 18.95–18.96 min (a), 19.04–19.06 min (b) and 19.23–19.27 min (c). CO_2 : F_2 = 50.7 kPa : 101.3 kPa, reaction temp. 498 K, and reaction time 50 h 21

Fig. 1.7. GC / EI–MS spectra of the products. (a) Total ion chromatogram, (b) mass chromatogram at m/z = 69, 66, 47 and 44, (c) mass spectra at the retention time of 9.02 min, (d) at the retention time of 9.15 min. CO_2 : F_2 = 50.7 kPa : 101.3 kPa, reaction temp. 498 K, reaction time 40 h, and GC oven temperature 223 K 23

Fig. 1.8. FT–IR spectra of products in the presence of CsF at various temperatures. CO_2 : F_2 = 76 kPa : 76 kPa, reaction time 50 h. Sampling amount 2 kPa (a) and 0.4 kPa (b) 25

Fig. 1.9. Mass chromatogram and MS spectra of the products in the presence of CsF. (a) Mass chromatogram at m/z = 69, 66 and 47, (b) mass spectra at the retention time of 9.04 min, (c) at the retention time of 9.17 min and (d) at the retention time of 9.39 min. CO_2 : F_2 = 76 kPa : 76 kPa, reaction temp. 498 K, reaction time 50 h, and GC oven temperature 223 K 26

Fig. 1.10. Mass chromatograms of the products obtained in the presence of CsF at (a) 303 K, (b) 423 K, (c) 473 K and (d) 498 K. CO_2 : F_2 = 76 kPa : 76 kPa, reaction time 50 h, and GC oven temperature 243 K 28

Fig. 1.11. Mass chromatogram of the products in the presence of CsF at the reaction temperature of 303 K. (a) Mass chromatograms at m/z = 69, 66 and 47 after (a)–1 0 and (a)–2 4 days. (b) Mass spectra of the sample in (a)–1 having the retention time of (b)–1 9.01 min, (b)–2 9.16 min, (b)–3 9.23 min and (b)–4 9.37 min. CO_2 : F_2 = 76 kPa : 76 kPa, reaction time 50 h, and GC oven temperature 223 K 29

Fig. 1.12. XPS F1s spectrum of CsF before and after the reaction. (a) Before reaction: (a)–1 non–etching and (a)–2 after etching; (b) after reaction: (b)–1 non–etching and (b)–2 after etching 30

Fig. 1.13. Yields of products in the direct reactions at various temperatures. CO_2 : F_2 = 76 kPa : 76 kPa and reaction time 50 h. (○) CF_2O, (△) CF_3OF, (□) CF_4, (◇) CF_3OOCF_3 and (×) $CF_2(OF)_2$ 33

Fig. 1.14. Yields of products in the presence of CsF at various temperatures. CO_2 : F_2 = 76 kPa : 76 kPa and reaction time 50 h. (○) CF_2O, (△) CF_3OF, (□) CF_4, (◇) CF_3OOCF_3 and (×) $CF_2(OF)_2$ 33

Fig. 1.15. Yields of products in the presence of EuF_3 at various temperatures. CO_2 : F_2 = 76 kPa : 76 kPa and reaction time 50 h. (○) CF_2O, (△) CF_3OF, (□) CF_4, (◇) CF_3OOCF_3 and (×) $CF_2(OF)_2$ 35

Fig. 1.16. Yields of products in the direct reaction at 498 K with various reaction times. CO_2 : F_2 = 76 kPa : 76 kPa. (○) CF_2O, (△) CF_3OF, (□) CF_4, (◇) CF_3OOCF_3 and (×) $CF_2(OF)_2$ 35

Fig. 2.1. Randles equivalent circuit and electric components 50

Fig. 2.2. Cole–Cole plot for Randles equivalent circuit 51

Fig. 2.3. Concept of the frequency response analyzer 53

Fig. 2.4. Schematic illustration of the original designed cell 56

Fig. 2.5. Schematic diagram of the CO_2 / F_2 electrochemical cell 57

Fig. 2.6. Schematic diagram of original line for electromotive force measurement. (1) CO_2 gas storage, (2) CO_2 gas cylinder, (3) F_2 gas storage, (4) F_2 gas cylinder, (5) cell for electromotive force, (6) F_2 gas pressure gauge, (7) F_2 gas pressure digital gauge, (8) CO_2 gas pressure gauge, (9) F_2 gas pressure gauge, (10) PIRANI gauge, (11) Ar gas cylinder, (12) gas sampler, (13) trap (liq. N_2), (14) vacuum pump (oil rotary), and (15) activated alumina 58

Fig. 2.7. XRD profiles of $PbSnF_4$ prepared at 273 K (a), 298 K (b) and 333 K (c), and reference (d) 59

Fig. 2.8. Rietveld refinement profile of $PbSnF_4$. (—: calculated, ●: observed, ○: difference), $R_F = 7.09$, $S = 9.1397$ 60

Fig. 2.9. Unit lattice of tetragonal $PbSnF_4$. $a_o = 0.4217$ nm, $c_o = 1.1427$ nm, Space group $P4/nmm$ 61

Fig. 2.10. Cole–Cole plot of tetragonal $PbSnF_4$ in air between 1 Hz and 500 kHz at 323 K. Sample thickness = 1 mm 63

Fig. 2.11. Electrical conductivity of tetragonal $PbSnF_4$ upon cooling from 473 K to 286K. (a) In air (◆), (b) in vacuum (■), (c) in Ar (●) and in Ar flow (▲), and reference values (d) (○) 64

Fig. 2.12. Chronoamperometry for $PbSnF_4$ at 373 K. Applied p.d. = 0.5 V (a), 0.1 V (b). Sample thickness = 1 mm 66

Fig. 2.13. The change in emf over time. Anode gas was 0.1 MPa CO_2 and cathode gas was χ MPa F_2 + (0.1 − χ) MPa Ar. (●: χ = 0.02, △: χ = 0.01) 68

Fig. 2.14. Cole–Cole plot of tetragonal $PbSnF_4$ between 1 Hz and 500 kHz at 373 K. (a) Anode and cathode gases were Ar, (b) anode gas was Ar, cathode gas was F_2 gas 69

List of Tables

Table 1.1. Some properties of the halogens 10

Table 1.2. Free energy data for halogens 12

Table 1.3. Yields of the products 32

Table 1.4. Formation rate of COF_2 and rate constant and activation energy of COF_2 formation 36

Table 2.1. Parameters for preparing $PbSnF_4$ in this study 54

Table 2.2. Atomic parameter by Rietveld analysis of $PbSnF_4$ 62

Table 2.3. Interatomic distance by Rietveld analysis of $PbSnF_4$ 62

Table 2.4. Conductivities taken by electron and hole, σ_e and σ_h in $PbSnF_4$ at 423 and 373 K 67

Scheme 1. The energy cycle with CO_2 fixing process 3, 14

Scheme 2. Scheme of competitive reaction processes. Blanketed compounds are the possible intermediates 43

Scheme 3. Some components of electrochemical impedance measurement for solid electrolyte 49

General Introduction

1 Global warming

In recent years, global warming has caused by the increase in concentration of carbon dioxide (CO_2) by consumption of fossil fuel and desertification with deforesting etc [1, 2].

Many chemical compounds found in the earth's atmosphere act as "greenhouse gases". When sunlight reaches the surface of the earth, some of the energy of the sunlight is reflected back towards space as infrared radiation (heat). Greenhouse gases absorb this infrared radiation and trap the heat in the atmosphere. This absorption causes the global warming.

The major natural greenhouse gases are water vapor, which causes about 36–70% of the greenhouse effect on Earth; carbon dioxide, which causes about 9–26%; methane, which causes about 4–9%, and ozone, which causes about 9–26% [3, 26–29]. The concentrations of several important greenhouse gases such as CO_2 have increased by about 25% since large–scale industrialization began around 150 years ago [4, 30–32]. The temperature of the atmosphere is climbing about 1.2 to 1.4° C since 1900.

Up to now, carbon dioxide has not been considered to be the important carbon resource so that the investigation about it has not been carried out enough. However, recently, from the point of view of the global environmental protection, many projects have been promoted from view of the possibility of recycling CO_2.

For this problem, the investigation on catalytic hydrogenation of carbon dioxide became important. It is examined to fix carbon dioxide by the photosynthesis due to plants and to synthesize methyl alcohol by hydrogen addition [5, 6]. These processes are based on the concept that carbon dioxide is final products of combustion. This is, carbon dioxide must be reduced by hydrogen to convert into methyl alcohol and hydrocarbon etc. Collected carbon dioxide reacts with hydrogen under the existence of a catalyst. It is converted to methyl alcohol and hydrocarbon etc., which can be used as a fuel.

The main reactions are shown as follows.

$$CO_2 + 3\ H_2 \rightarrow CH_3OH + H_2O$$

$$CO_2 + 4\ H_2 \rightarrow CH_4 + 2\ H_2O$$

The investigation on methyl alcohol synthesis is carried out most actively in the field of the catalytic hydrogenation of carbon dioxide. According to the report by T. Inui et al [7], they developed the Cu–Zn–Cr–Al_2O_3 catalyst with very high activity. When Pb and Ag were added to Cu–Zn–Cr–Al_2O_3 catalyst, the conversion ratio from carbon dioxide to methyl alcohol became 22.1% at 523 K, 50 atm.

In the catalytic hydrogenation of carbon dioxide, methane is the main product. According to the report by T. Inui et al [8], in methanation of carbon dioxide, they developed the catalyst of Ni–Ru–La_2O_3 system. In this case, the conversion ratio of carbon dioxide became 100% at 523 K.

2 Reaction between CO_2 and F_2

From the point of view concerning to fluorine chemistry, what can be done to contribute to the carbon dioxide fixation? The elementary fluorine has the strongest

oxidizing ability (E_0 = 2.87 V) among all elements and it is only the element that can oxidize the oxides [9, 10]. For instance, alumina is one of the most stable oxides. But even the alumina is fluorinated with heat radiation, and oxygen is isolated.

Using elementary fluorine, the energy cycle in which carbon dioxide is used as a fuel will be able to propose. One example of this new energy cycle including the reaction between CO_2 and F_2 is shown in scheme 1.

First, CO_2 is converted to COF_2 by the reaction between CO_2 and F_2. During this process, O_2 and the energy may be generated [11]. Next, COF_2 is used to produce the carbonate compound as a reagent of organic synthesis with alcohols, thereby producing HF. The HF is converted into fluorine gas by electrolysis. Hydrogen gas is a by–product here. The solar energy can be used for this electrolysis and hydrogen is also the one of the key–fuel for the energy in the future.

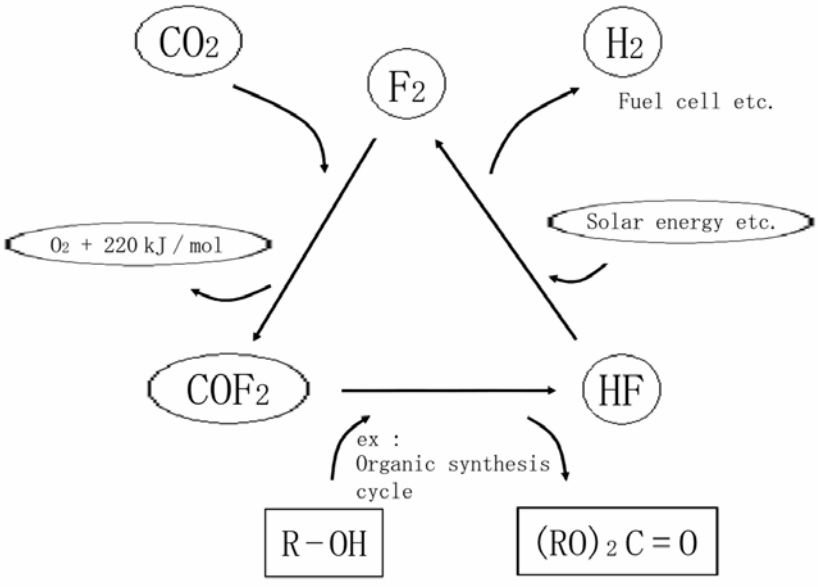

Scheme 1. The energy cycle with CO_2 fixing process.

The reaction between CO_2 and F_2 to form COF_2 must take place spontaneously even at room temperature because the Gibbs free energy change of the reaction is calculated as – 220 kJ mol^{-1} [11].

$$CO_2 + F_2 \rightarrow COF_2 + 1/2\ O_2 + (-\Delta G)\ 220\ \text{kJ mol}^{-1}$$

The theoretical electromotive force calculated from its Gibbs free energy is 1.14 V, which value is mostly equal to the electromotive force 1.23 V of the H_2 / O_2 fuel cell [12, 13].

There has been no investigation based on this concept. In order to examine the possibility of establishment of this energy cycle including the CO_2 / F_2 fuel cell for fixation of CO_2, at first, a safe apparatus in which the reaction took place is constructed.

We have tried to examine the CO_2 / F_2 electrochemical cell with $PbSnF_4$ as one device for the fixation of CO_2. At same time, this cell is a device that converts the chemical energy of the reaction between CO_2 and F_2 into electrical energy.

Tetragonal $PbSnF_4$ [14–18] is known as a fluoride ion conductor having high electric conductivity at ambient temperatures, and $PbSnF_4$ has been used for the design of chemical sensors, and operated as oxygen sensors [19–21] from room temperature up to 523 K.

COF_2 has not been used for the variety of applications. However, during the last three decades, carbonyl fluoride (COF_2) plays a key role in both atmospheric and plasma etching chemistry and flame suppression behavior of fluorocarbons. COF_2 and fluorooxomethyl radical ($FCO^{\bullet}$) are important intermediates [22, 23] in the oxidative degradation of many fluorinated compounds. These species are involved in the mechanism of flame suppression by the fluorinated compounds. These species are also formed in the fluorocarbon / oxygen plasma used in many etching processes.

Perfluorocompounds (PFCs) are mainly used as the etching gas for the etching process and as the cleaning gas of chemical vapor deposition chamber in semiconductor manufacturing. It is reported that PFCs have large effect on global warming by the greenhouse effect, because they have very long atmospheric lifetimes. Many governments of the world decided to conclude the Kyoto Protocol [33]. Japan will be obliged to reduce greenhouse gases by 6% compared to the base year of 1990. Numerous studies have been performed on reducing PFCs emissions. The development of several gases, such as COF_2 and F_2, has shown promising results. Many semiconductor companies have been adopted COF_2 in terms of reducing the global warming impact. COF_2 has a small global warming potential, because hydrolysis proceeds rapidly, even in the atmosphere, to give CO_2 and HF.

3 Objective of this study

This study reports the reaction between carbon dioxide and elementary fluorine [24, 25]. The main objective of studying this reaction was to construct the CO_2 / F_2 electrochemical cell with $PbSnF_4$ as one of the methods for the fixation of CO_2.

This study consists of 3 chapters. Chapter 1 is directly concerned with the reaction between CO_2 and F_2 as an approach to a CO_2 / F_2 fuel cell. The properties of fluorine, the reactions with CO_2 and the concept of new energy cycle are described in Chapter 1.1 as introduction. The experimental method such as the construction of reaction apparatus, experimental procedure, and analysis of products are presented in Chapter 1.2. Results and discussion are presented in Chapter 1.3.

In chapter 2 based upon the results in chapter 1, the CO_2 / F_2 electrochemical cell as the device for the fixation of CO_2 was reviewed. The chapter 2.1 consists of a theory and

the device as the CO_2 / F_2 fuel cell. The preparation of $PbSnF_4$ as the solid electrolyte, experimental procedures, analysis of products, and the construction of electrochemical cell as one of the methods for the fixation of CO_2 are presented in Chapter 2.2. The structure and electrochemical properties of tetragonal $PbSnF_4$, and an electrochemical cell performance are discussed in Chapter 2.3. The measurement of electron motive force, the preparation of COF_2 in a CO_2 / F_2 electrochemical cell, and its results were mentioned.

Finally, conclusions and future work are presented in Chapter 3.

References and Notes

[1] Iwao Omae, Nisankatannso to Tikyukankyou, Tyukousinnsho (1999) pp. 23–142. http://cdiac.esd.ornl.gov/trens/emis/em_cont.htm.

[2] J. Houghton, Grobal Warming: The Complete Briefing, Cambridge University Press, New York, NY (1997).

[3] P. M. Vitousek, Ecology 75 (1994) 1861–1876.

[4] IPCC Third Assessment Report: Climate Change 2001.

[5] Y. Matsumoto, M. Obata, and J. Hombo, J. Phys. Chem. 98 (1994) 2950–2951.

[6] W. M. Sears and S. R. Morrison, J. Phys. Chem. 89 (1985) 3295–3298.

[7] T. Inui, T. Takeguchi, Catal. Today 10 (1991) 95–106.

[8] T. Inui, M. Funabiki, Y. Sezume, J. Chem. Soc. Faraday Trans 175 (1979) 787–802.

[9] P. Politzer, J. Am. Chem. Soc. 91 (1969) 6235–6237.

[10] The Entrance of Fluorine Chemistry, 155 Committee of Fluorine Chemistry. (Printed in Japan, 1999)

[11] J. C. Amphlett, J. R. Dacey, G. O. Pritchard, J. Phys. Chem. 75 (1971) 3024–3026.

[12] Gregor Hoogers, Fuel Cell Technology Handbook (CRC press, 2003).

[13] W. M. Latimer, The Oxidation States of the Elements and Their Potentials in Aqueous Solutions (Prentice Hall, New York, 1952).

[14] D. J. Donaldson, B. J. Senior, J. Chem. Soc. (A) 1821–1825 (1967).

[15] J. M. Reau, C. Lucat, J. Portior, P. Hagenmuller, L. Cot, S. Vilminot, Mat. Res. Bull. 13 (1978)877–882.

[16] J. Pannetier, G. Denes, J. Lucas, Mat. Res. Bull. 14 (1979) 627–631.

[17] G. Perez, S. Vimont, W. Granier, L. Cot, C. Lucat, J. M. Reau, J. Portior, P. Hagenmuller, Mat. Res. Bull. 15 (1980) 587–593.

[18] G. Denes, M. C. Madamda, A. Muntasar, A. Peroutka, K. Tam, and Z. Zhu, Nato, Sci. Ser. 25–38 (1999).

[19] A. Wakagi, J. Kuwano, Y. Saito, J. Mat. Chem. 41 (1994) 973–975.

[20] T. Eguti, S. Suda,T. Hijii, S. Koga, J. Kuwano, Y. Saito, Key Engineering Materials. 181–182 (2000) 199–202.

[21] A. Wakagi, J. Kuwano, M. Kato, H. Hanamoto, Solid State Ionics, 70–71 (1994) 601–605.

[22] M. R. Zachariah, W. Tsang, P. R. Westmoreland, D. R. F. Burgess, J. Phys. Chem. 99 (1995) 12512–12519.

[23] T. J. Burckley, R. D. Johson, R. E. Hule, Z. Zhang, S. C. Kuo, and R. B. Klemm, J. Phys. Chem. 99 (1995) 4879–4885.

[24] Yasuo Hasegawa, Reiko Otani, Susumu Yonezawa, Masayuki Takashima, J. Fluorine Chem. 128 (2007) 17–28.

[25] Yasuo Hasegawa, Akitomo Nagasaka, Jae–Ho Kim, Susumu Yonezawa, Masayuki Takashima, J. Fluorine Chem. 128 (2007) 958–964.

Hp Reference site on the internet

[26] http://www.epa.gov/airmakets/climtchg/index.html.

[27] http://yosemite.epa.gov/org/globalwarming.nsf/content/emissions.html.

[28] http://www.atmo.arizona.edu/students/courselinks/spring04/atmo451b/pdf/

Radiation Budget.pdf.

[29] http://www.realclimate.org/index.php?p–142.

[30] http://www.eia.doe.gov/oiaf/1605/ggccebro/chapter1.htlm

[31] http://www.grida.no/climate/ipcc_tar/wg1/016.htm.

[32] http://www.grida.no/climate/ipcc_tar/wg1/fig6–6.htm.

[33] http://www.runfccc.de/index.html.

Chapter 1

Reaction between carbon dioxide and elementary fluorine

1.1. Introduction

The reaction between CO_2 and F_2 to form COF_2 takes place spontaneously even at room temperature because the Gibbs free energy change of the reaction is calculated as –220 kJ mol^{-1} [1].

$$CO_2 + F_2 \rightarrow COF_2 + 1/2\ O_2 + (-\ \Delta G\ )\ 220\ kJ\ mol^{-1}$$

Some reports have addressed preparation of COF_2 [2, 3] and CF_3OF [2] from CO and F_2; few reports have examined the reaction between CO_2 and F_2. Only three reports have described formation not of COF_2, but of $CF_2(OF)_2$, using CsF as a catalyst [4–6]. To confirm the conversion of CO_2 into COF_2, the reaction between CO_2 and F_2 has been tried at various temperatures from 303 to 523 K under various pressure and mixing ratios of both gases. This reaction was carried out similarly in the presence of NaF, CsF and EuF_3. Catalytic abilities of these metal fluorides to form COF_2 were examined. In addition, the reaction mechanism and reaction rate are discussed in this paper.

1.1.1 Properties of fluorine

Although the chemistry of the halogens is somewhat complex, similarities within the group are more pronounced than in any of the other groups. The elements, fluorine, chlorine, bromine, iodine, and astatine, are collectively called halogens, or salt producers, because they all have high electronegativity (F = 4.0, Cl = 3.0, Br = 2.8, I = 2.5) and form negative halide ions such as ionic salts. Except for fluorine, they also show positive oxidation states. Because of their high electronegativity, the halogens show practically no metallic properties. Fluorine has the largest electronegativity of all the elements. Therefore, it can show only a negative oxidation state. The other halogens show positive oxidation states in compounds with more electronegative elements.

Fluorine [7, 8] exhibits a number of anomalous properties, both as an atom and as a molecule. Some properties of the group are shown in table 1.1. As indicated by the relatively high values of the ionization potentials, it is fairly difficult to remove an electron from a halogen atom. Within the group from F_2 to I_2, there is a decrease in the ionization potentials.

Table 1.1

Some properties of the halogens

Halogen	Melting point ℃	Boiling point ℃	Ionaization potential eV	Electron affinity eV	Atomic radius Å	Oxidation potential volts (X^- to X_2)	Dissosiation energy of molecule kcal mol^{-1}
F	-223	-187	17.42	3.448	0.5741	-2.87	37
Cl	-102	-34.6	13.01	3.613	0.9748	-1.36	57.88
Br	-7.3	58.78	11.84	3.363	1.0117	-1.09	45.92
I	114	183	10.44	3.063	1.324	-0.54	35.86

The ionization potentials show the monotonic increase in going from iodine to fluorine. The electron affinities of iodine, bromine, and chlorine also increase gradually. In fact, there is a liner correlation between ionization potential and electron affinity for these three elements. The electron affinity of fluorine deviates very markedly from the general trend, and it is less than that of chlorine. This deviation can be obtained by extrapolating the liner relationship to the ionization potential of fluorine. It corresponds to an electron affinity of 4.59 eV, which is 1.14 eV (26.3 kcal mol^{-1}) greater than the true value. Thus, the electron affinity of fluorine is estimated to be 1.14 eV greater than the true value.

Apparently, the formation of the fluoride ion includes an unusual destabilizing effect corresponding to about 26.3 kcal mol^{-1}. For example, there should be observed a corresponding lowering of the bond energies of the metal fluoride.

The metal fluorides are considered to be ionic, and the bond energies of the fluorides are consistently lower about 26.3 kcal mol^{-1} among the other halides. The dissociation energy of F_2 is very low, relative to the trend among the other halogen molecules.

Although the bond between the halogen atoms in the X_2 molecules is fairly strong as shown in table 1.2, the attraction between X_2 molecules is quite weak and due only to van der Waals forces. It would be expected van der Waals attraction to increase with increasing number of electrons per X_2 molecules. Thus, the boiling points increase in going from F_2 to I_2.

The oxidation potentials are greatly significant. The potentials show that fluorine gas is the best oxidizing agent of the group. The reason for this is not so simple as it appears. The overall half–reaction can be constructed from the alternate path:

$$X^- (aq) \rightarrow 1/2\ X_2 (g) + e^-$$

$$X^- (aq) \rightarrow X^- (g) \rightarrow X (g) + e^- \rightarrow 1/2\ X_2 (g) + e^-$$

The free energy changes for various steps are listed in table 1.2. In the case of fluorine, the sum of the three processes shown has a net free energy change of + 182 kcal for $X^- (aq) \rightarrow 1/2\ X_2 (g) + e^-$. The electron is referred to a hydrogen electrode standard, which amounts to having a change of – 115 kcal in the free energy.

$$X^- (aq) + H^+ \rightarrow 1/2\ X_2 (g) + 1/2\ H_2 (g) + (\Delta G)\ 67\ \text{kcal mol}^{-1}$$

By using the relation $\Delta G° = – nFE°$, the calculated oxidation potential for fluorine is – 2.87 volts.

Table 1.2

Free energy data for halogens (kcal mol^{-1})

Step	Fluorine	Chlorine	Bromine	Iodine
$X^-(aq) \rightarrow X^-(g)$	114	84	78	70
$X^-(g) \rightarrow X(g) + e^-$	83	86	81	74
$X(g) \rightarrow 1/2\ X_2(g)$	-15	-25	-19	-14

Comparing the halogens with each other, there is a large increase in ionic radius (1.33 Å for F^-, 1.81 Å for Cl^-, 1.96 Å for Br^-, and 2.20 Å for I^-) from F^- to I^-. The reason why F_2 is a good oxidizing and reactive agent is that the fluoride ion is so small such as hydrogen. The smaller size of the fluoride ion leads to more favorable lattice energies.

The fields of fluorine chemistry lie at the boundary between organic and inorganic chemistry. Inorganic fluorine chemistry is concerned with the productions and the

reactions of a wide variety of volatile and nonvolatile inorganic compounds which are prepared through various fluorination processes. Some of these fluorinated inorganic compounds have been used often as fluorinating reagents. Most volatile inorganic fluorides are prepared with using elemental fluorine, either directly or through the reactions with fluorinating reagents such as ClF_3. The strong tendency of inorganic fluorides to form salts, complexes, and coordination compounds leads to a wide variety of nonvolatile inorganic fluorine compounds.

1.1.2 New energy cycle with CO_2 fixing process

A strong oxidant, F_2 can oxidize the oxides. Previously, we have reported a reaction between CO_2 and F_2 to form COF_2 [9–11]. By this reaction, CO_2 can be converted to COF_2. The Gibbs free energy change of this reaction is calculated as – 220 kJ mol^{-1} [1]. Furthermore, the theoretical electromotive force calculated from its Gibbs free energy is 1.14 V, which value is mostly equal to the electromotive force 1.23 V of the H_2 / O_2 fuel cell [12, 13].

As described above, we proposed one example of this new energy cycle including the reaction between CO_2 and F_2 in scheme 1.

To complete this cycle, the reaction between CO_2 and F_2 must be investigated in detail. Finally, based on this idea, we tried to investigate COF_2 formation using CO_2 and F_2 in the electrochemical cell with $PbSnF_4$ as one method for CO_2 fixation.

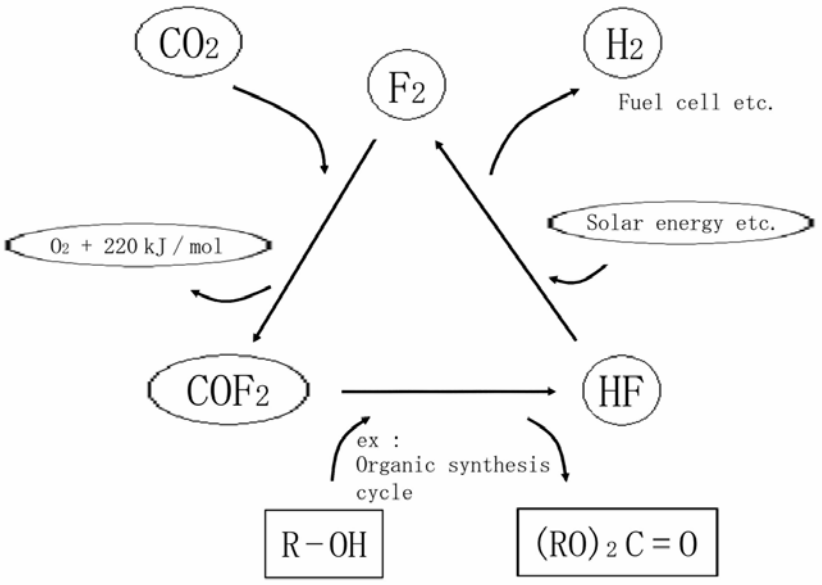

Scheme 1. The energy cycle with CO_2 fixing process.

1.2. Experimental

Fig. 1.1 shows a gas line made of SUS 316L for the reaction between CO_2 and F_2, which was originally designed to control and monitor reaction pressures and temperatures precisely. This apparatus has three separate parts: a gas–gas reaction line, a trap–to–trap separation line, and a vacuum line.

The reactor was filled with F_2 gas at 20 kPa; it was kept at 523 K for one day to passivate the inner wall of the line before use. The F_2 gas in the exhaust was eliminated by passing it through the activated alumina column. The reactor vessel capacities were 59.6 ml. The amount of F_2 gas that was fixed to the activated alumina was about 300 dm^3 / 450 g Al_2O_3.

The CO_2 was introduced into the reactor and the reactor was cooled to 77 K (liquid

N_2). Then, F_2 gas was introduced into the reactor. The reaction temperature was controlled at 303–523 K. Residual F_2 in the product was eliminated by vaporization at 77 K.

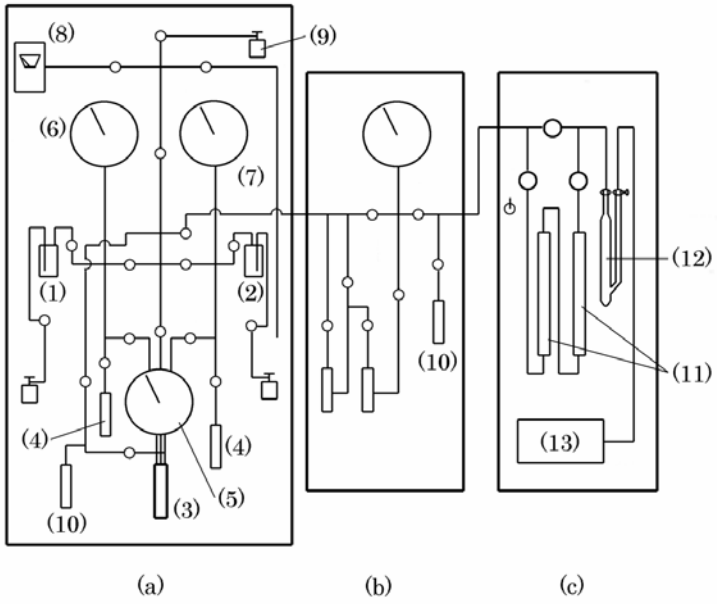

Fig. 1.1. Apparatus for the reaction between CO_2 and F_2. (a) Gas–gas reaction line, (b) trap–to–trap separation line and (c) vacuum line. (1) CO_2 gas storage, (2) F_2 gas storage, (3) reactor (SUS316L), (4) constant volume container, (5) reactor pressure gauge, (6) CO_2 gas pressure gauge, (7) F_2 gas pressure gauge, (8) PIRANI gauge, (9) Ar or He gas cylinder, (10) gas sampler, (11) activated alumina, (12) trap (liquid N_2), and (13) vacuum pump (oil rotary).

For the reaction with the metal fluorides, the metal fluoride (1 equiv. mol or 3 g) was

first put into a nickel container. Before use, the metal fluorides were kept all through the night in F_2 gas at 503 K to eliminate trace amounts of water and oxides.

After mixing CO_2 and F_2, the temperature at the surface of the reactor was measured. The relation between the lapse of time and pressure change was measured to monitor the reaction progress. The total pressure was fixed at 152 kPa.

The reaction product after eliminating F_2 was introduced into the 10 cm path length IR cell having BaF_2 or CaF_2 window at 2 kPa or 0.4 kPa (FT–IR 8960 PC; Shimadzu Corp.). Moreover, the product was analyzed by GC / FT–IR (Nexus; Thermo Nicolet Japan Inc.) with a sample amount 20 μl, split–less and GC / EI–MS, CI–MS: for EI (6890 / 5970 GC / MDS; Hewlett Packard Co.), m/z 15–300, with a sample amount 20 μl, splitless; for CI with methane, (QP 5000A; Shimadzu Corp.), m/z 45–300, with a sample amount 1 ml, split). The capillary column for the GC was 100 m (for GC / FT–IR, 200 m) × 0.25 mm × 0.5 μm (DB–PETRO; J&W Scientific Inc.). The oven temperature was controlled at 223, 243 and 303 K. Before GC / MS analysis, helium gas was introduced into the reactor so that the total pressure was set at 202.6 kPa.

The calibration line of the reaction product was prepared with IR data and MS intensity.

Fig. 1.2(a) portrays a CO_2 calibration line in which the absorbance was plotted against the pressure. Into the IR cell, CO_2 gas was introduced at a proper pressure; the IR spectra were measured at resolution of 4 cm^{-1}. The absorption peak at 2360 cm^{-1} was chosen for the calibration line of CO_2. For COF_2, CF_3OF, $CF_2(OF)_2$ and CF_3OOCF_3 [2], the relations between the pressure and the absorbance were referred from the literature [4, 14–19]. The calibration line was obtained by plotting the absorbance against the pressure. Fig. 1.2(b) shows the COF_2 calibration line. Line 1 in Fig. 1.2(b) was drawn using the absorbance at 1930 cm^{-1} in the literature [17]. The corrected

calibration line, line 2 in Fig. 1.2(b) was obtained by plotting the absorbance against the pressure measured by Central Glass Co. Ltd. [18]. The slopes of line 1 and line 2 were approximated respectively as 1803, 1254. Fig. 1.2(c) shows the CF_3OF calibration line. Line 1 in Fig. 1.2(c) was drawn using the absorbance at 1282 cm^{-1} in the literature [19]. However, the sum of CO_2 residual pressure and pressure of CF_3OF was greater than 2 kPa, which was the total pressure at the measurement, when the pressure of CF_3OF was estimated using line 1 in Fig. 1.2(c). The corrected calibration line 2 was determined by considering the effect of IR spectrum resolution against line 1. The slopes of line 1 and line 2 were respectively approximately 366, 153. The pressures evaluated using these corrected calibration lines were about 50% lower than those by calibration lines with plotting the values in the literature [4, 14–17, 19]. In this case, the resolution greatly affected the absorption intensity. Line 3 in Fig. 1.2(c) was obtained by plotting the absorbance at 945 cm^{-1} against the pressure. Line 3 was used instead of line 2 when the absorbance at 1282 cm^{-1} could not be used for the calculation.

Fig. 1.2(d) is the CF_4 calibration line. This line plotted the MS intensity against concentration of CF_4. The concentration of CF_4 and its MS intensity were measured using GC / MS with the standard sample. The CF_4 concentration was measured as a volume percentage of the GC injection gas. It was assumed that the MS intensities of COF_2 and CF_3OOCF_3 were equal to that of CF_4 to draw the calibration line of COF_2 and CF_3OOCF_3.

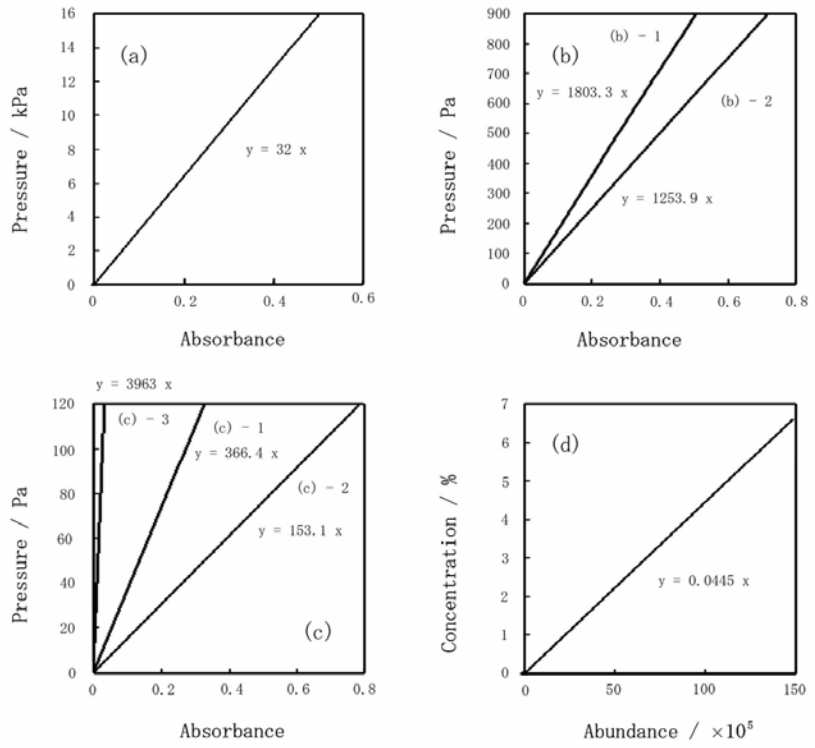

Fig. 1.2. Calibration lines of CO_2 (a), COF_2 (b), CF_3OF (c) and CF_4 (d). (b)–1 and (b)–2 correspond, respectively, to data at 1930 cm^{-1} in Ref. [17] and Ref. [18]. (c)–1, (c)–2 and (c)–3 correspond to data at 1282 cm^{-1} in Ref. [19], at 1282 and at 945 cm^{-1} measured in this study.

1.3. Results and Discussion

1.3.1. Reaction product

The pressure change was observed obviously with increasing reaction time as shown in Fig. 1.3.

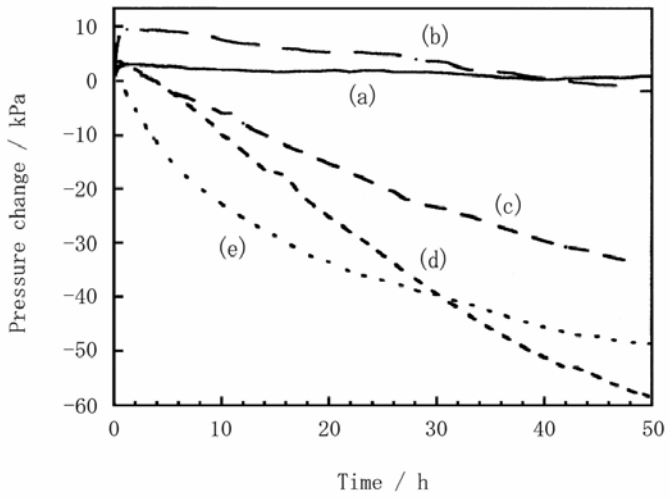

Fig. 1.3. Transient of the pressure change in the direct reactions at (a) 373 K, (b) 423 K, (c) 473 K, (d) 498 K and (e) 523 K. CO_2 : F_2 = 50.7 kPa : 101.3 kPa and reaction time 50 h.

Fig. 1.4 shows FT–IR spectra of the reaction products of the direct reaction of CO_2 and F_2 have many peaks. The absorption peaks corresponded to O–F, C–F and CF=O bonds that appeared respectively at 800–1000 cm^{-1}, 1200–1300 cm^{-1}, and around 1930 cm^{-1}. The absorption peaks at 2360 and 3700 cm^{-1} indicate the presence of residual CO_2. Some fluorocarbon compounds, including CF_3OF, were inferred to have been produced.

Gram–Schmide spectra of the reaction product measured using GC / FT–IR are shown in Fig. 1.5. They confirmed that three products existed, with retention times of 18.95–18.96, 19.04–19.06 and 19.23–19.27 min.

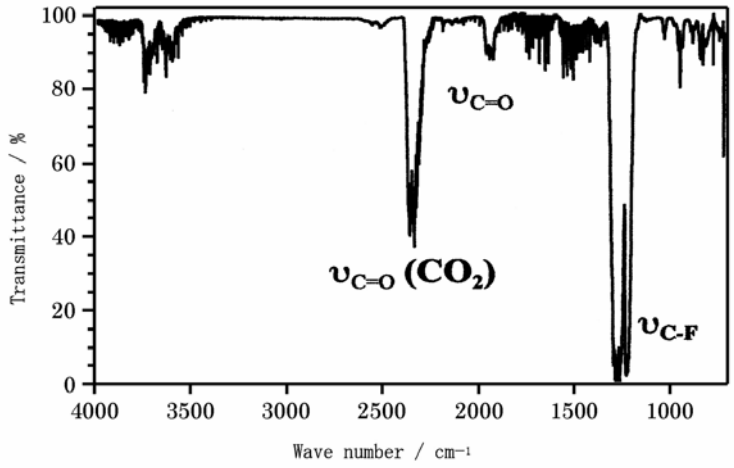

Fig. 1.4. FT–IR spectrum of the product in the direct reaction. CO_2 : F_2 = 76 kPa : 76 kPa, reaction temp. 498 K, and reaction time 24 h.

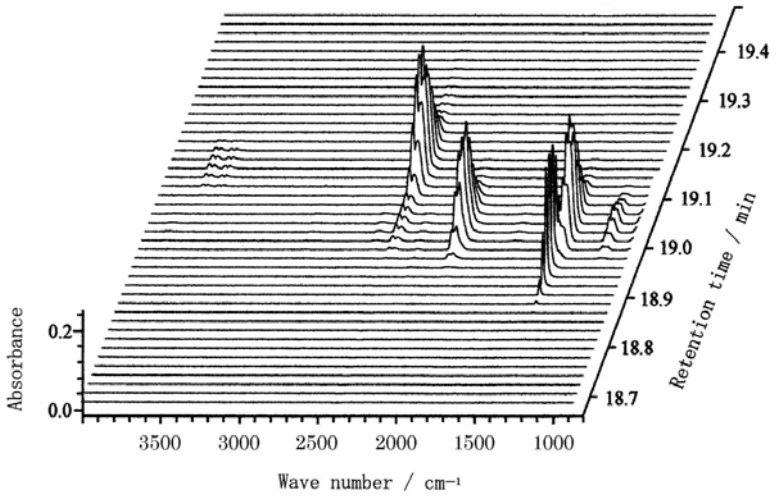

Fig. 1.5. Gram–Schmide spectra of the product measured using GC / FT–IR. CO_2 : F_2 = 50.7 kPa : 101.3 kPa, reaction temp. 498 K, and reaction time 50 h.

The IR spectra of the products separated by GC / FT–IR are shown in Fig. 1.6. IR spectra of the product sampled at the retention times of 18.95–18.96, 19.04–19.06 and 19.23–19.27 min are also shown in Figs. 1.6(a)–(c). Fig. 1.6(a) shows that the product with retention time of 18.95–18.96 min had a characteristic absorption peak at 1282 cm^{-1} corresponding to a C–F bond.

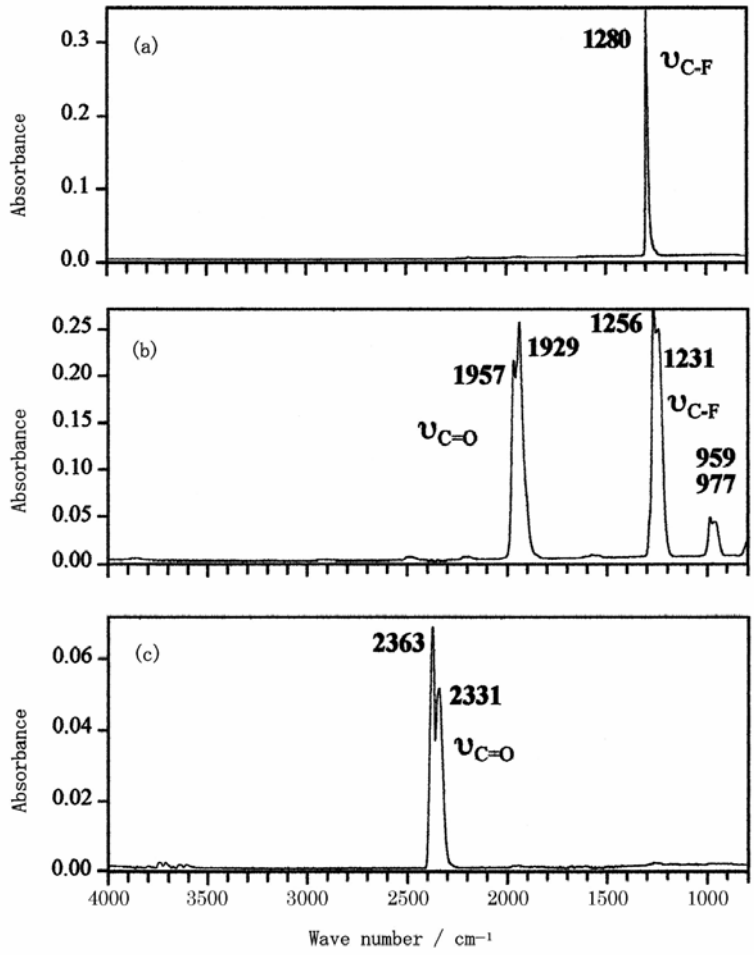

Fig. 1.6. GC / FT–IR spectra of the products at retention times of 18.95–18.96 min (a), 19.04–19.06 min (b) and 19.23–19.27 min (c). CO_2 : F_2 = 50.7 kPa : 101.3 kPa, reaction temp. 498 K, and reaction time 50 h.

Similarly, the product with retention time of 19.04–19.06 min had characteristic absorption peaks at 1929 cm^{-1} (CF=O), 1256 cm^{-1} (C–F) and 977 cm^{-1} (C－F), as shown in Fig. 1.6(b), and the product with the retention time of 19.23–19.27 min had characteristic absorption peaks at 2331 cm^{-1} (CO_2), 2361 cm^{-1} (CO_2) and 3700 cm^{-1} (CO_2), as shown in Fig. 1.6(c). Matching with HR Nicolet Vapor Phase Library (Thermo Nicolet Japan Inc.) revealed that the respective products were CF_4 [20], COF_2 [21] and CO_2.

Fig. 1.7 shows the total ion chromatogram of the gaseous reaction product and GC / MS spectra in the direct reaction. Three peaks existed at the retention times of 9.02, 9.15 and 9.45 min. The numbers in the figure indicate the m/z values. Fig. 1.7(b) shows the mass chromatogram of m/z = 69, 47, 66 and 44. Ions with m/z = 69, 47, 66 and 44 corresponded, respectively, to CF_3^+, COF^+, COF_2^+ and CO_2^+ [9]. Fig. 1.7(c) and (d) were mass spectra of the products sampled at 9.02 and 9.15 min, where the peaks attributable to N_2 and O_2 were subtracted as a background. However, as shown in Fig. 1.7(c), one ion indicated m/z = 32 because the oxygen in air mixed with the sample injection could not be subtracted sufficiently. The ion with m/z = 69, corresponding to CF_3^+ was detected at the retention time of 9.02 min; ions with m/z = 47 and 66 corresponding to COF^+ and COF_2^+ were detected at the retention time of 9.15 min. Comparing the spectra to the data in NIST Library, the MS spectra at 9.02 and 9.15 min correctly corresponded, respectively, to CF_4 [20], COF_2 [21]. In addition, the result of positive CI–MS also suggested that CF_4 [20] and COF_2 [21] were produced.

It is noteworthy that the ions with m/z = 85 and 54 corresponding, respectively, to CF_3O^+ and OF_2^+ were not observed by GC / MS analysis. However, CF_3OF was confirmed by FT–IR spectra, as shown in Fig. 1.4. The characteristic absorption peak corresponding to OF_2 was also observed at 860 cm^{-1}. Moreover, CF_3OF and OF_2 were

not observed by GC / FT–IR and GC / MS [23] because these products had adsorbed on the column strongly and reacted with the column. Some fluorocompounds, such as CH_3SiF_3, $(CH_3)_2SiF_2$ and fluorobenzene, were detected during measurements.

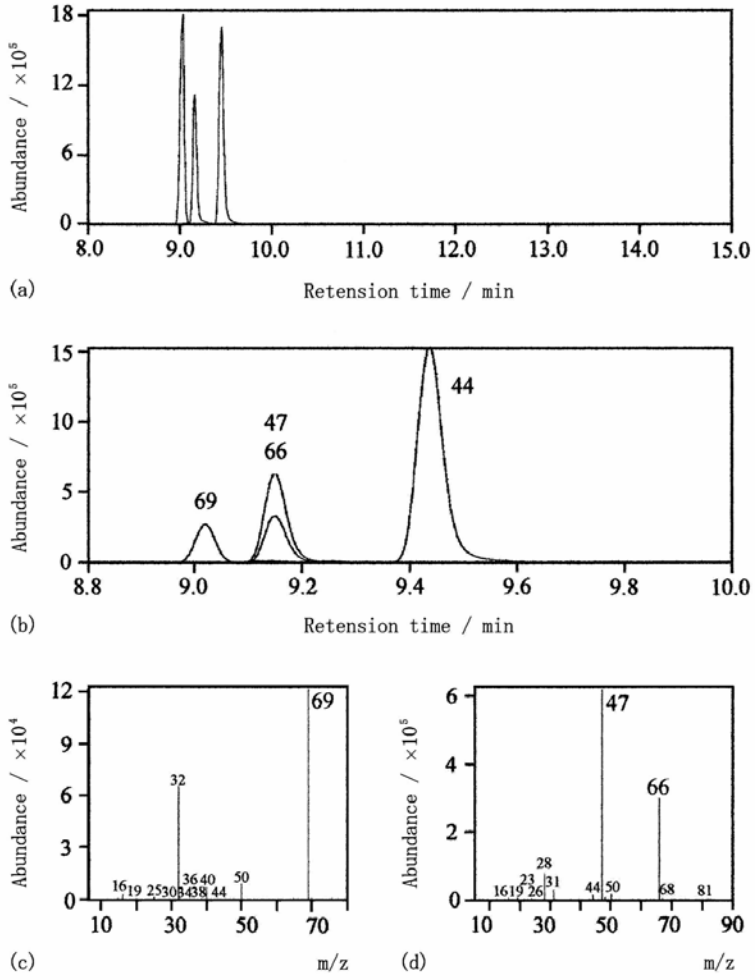

Fig. 1.7. GC / EI–MS spectra of the products. (a) Total ion chromatogram, (b) mass chromatogram at m/z = 69, 66, 47 and 44, (c) mass spectra at the retention time of 9.02 min, (d) at the retention time of 9.15 min. CO_2 : F_2 = 50.7 kPa : 101.3 kPa, reaction temp. 498 K, reaction time 40 h, and GC oven temperature 223 K.

Results show that CF_3OF, COF_2 and CF_4 were the major products of the direct reaction between CO_2 and F_2 around 473 K. It is noteworthy that the reaction between CO_2 and F_2 proceeded very slowly at room temperature. Confirmation of the CF_3OOCF_3 formation was not possible in the direct reaction. The generated OF_2 at the reaction, along with F_2, was eliminated by vaporization at 77 K. Little OF_2 remained in the product.

1.3.2. In the presence of metal fluorides

Reaction between CO_2 and F_2 n the presence of metal fluoride was carried out under various conditions. In the presence of NaF and EuF_3, the results of this reaction were similar to that of the direct reaction. However, the FT–IR spectrum of the reaction in the presence of CsF differed from that in the absence of metal fluoride and the presence of EuF_3 and NaF.

The FT–IR spectra of the reaction product in the presence of 3 g (2×10^{-2} mol) CsF are shown in Fig. 1.8. The shape of the absorption profile changed between 1100 and 1300 cm^{-1}. Absorption peaks at 1167 and 1202 cm^{-1} newly appeared and the absorption peak at 1285 cm^{-1} shifted to 1289 cm^{-1}. Fig. 1.8(b) shows that the reaction product was clearly different at each reaction temperature. In the case reacted at 303 K, the product displayed strong absorption peaks at 1267, 1248, 1202, 1186 cm^{-1}, etc. The strong peak at 1202 cm^{-1} became weak at temperatures over 373 K. The amount of the product having this strong peak decreased with increasing temperature. It disappeared completely at 473 K. On the other hand, the strong peak of 1167 cm^{-1} appeared clearly at 498 K. Strong absorption peaks at 1267, 1248, 1202, 1186 cm^{-1}, etc. were attributed to $CF_2(OF)_2$ [14]. At high temperatures over 373 K, the amount of CF_3OF in the products

increased at an increasing rate [24]. Moreover, the peak at 1167 cm^{-1} appeared at 498 K and was identified as that of CF_3OOCF_3 [15, 16].

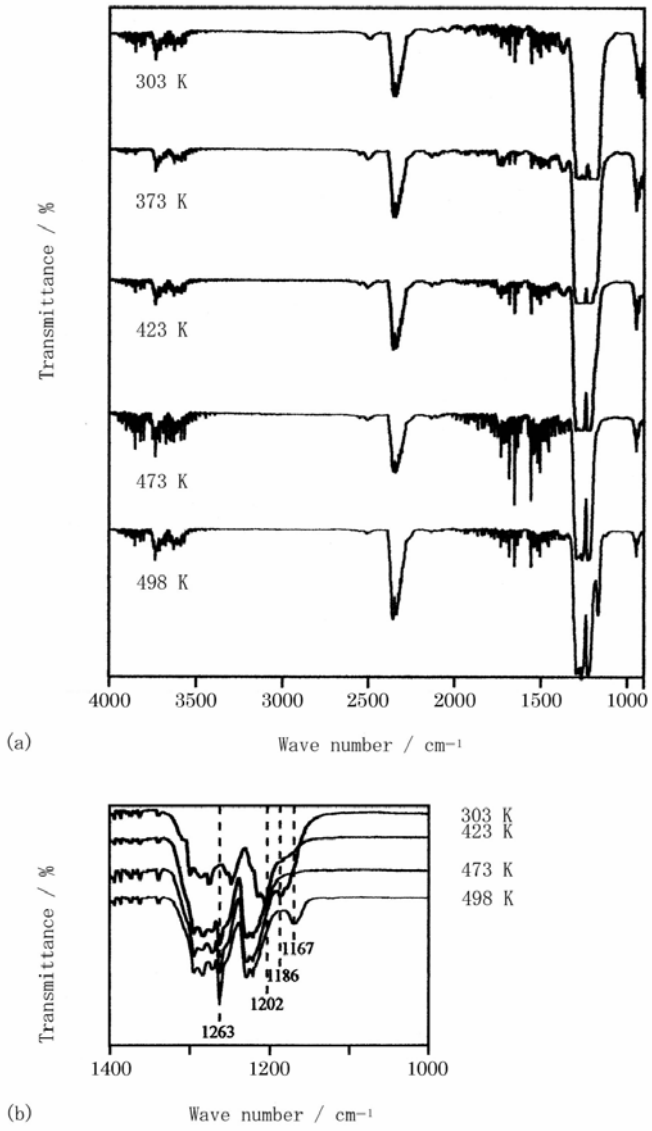

Fig. 1.8. FT–IR spectra of products in the presence of CsF at various temperatures. CO_2 : F_2 = 76 kPa : 76 kPa, reaction time 50 h. Sampling amount 2 kPa (a) and 0.4 kPa (b).

In the presence of 260 mg (1.65×10^{-3} mole) CsF at various temperatures, CF_3OF and OF_2 formed and $CF_2(OF)_2$ did not form, even at 303 K. The result was similar to that of the direct reaction when the amount of CsF was small.

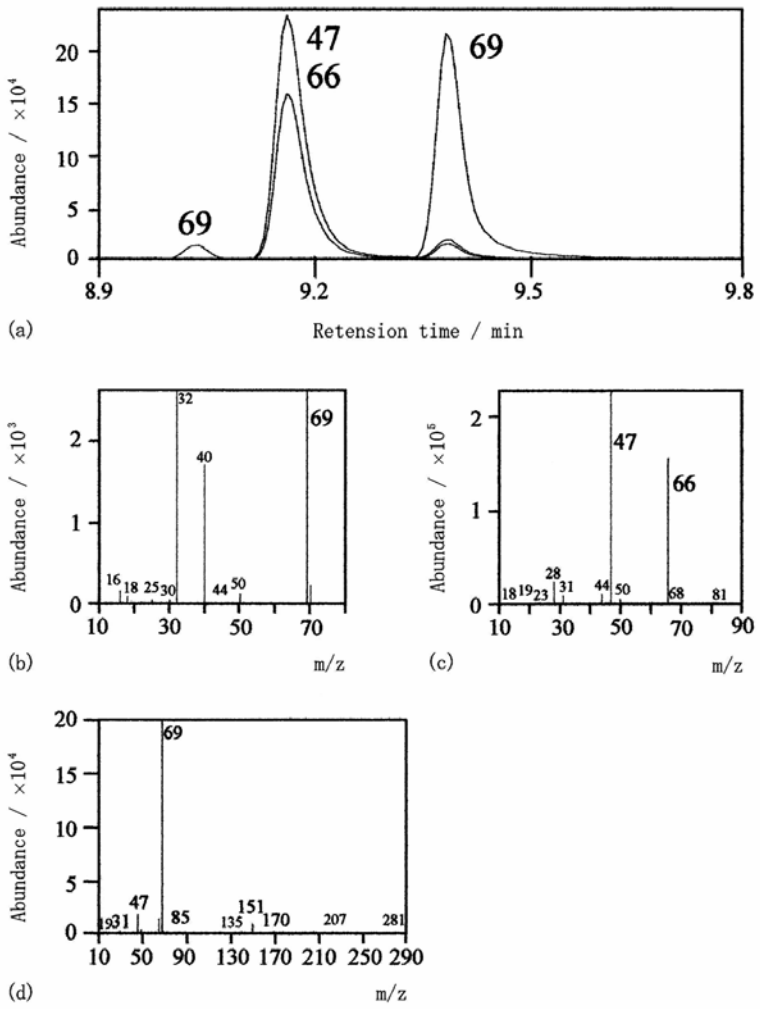

Fig. 1.9. Mass chromatogram and MS spectra of the products in the presence of CsF. (a) Mass chromatogram at m/z = 69, 66 and 47, (b) mass spectra at the retention time of 9.04 min, (c) at the retention time of 9.17 min and (d) at the retention time of 9.39 min. CO_2 : F_2 = 76 kPa : 76 kPa, reaction temp. 498 K, reaction time 50 h, and GC oven temperature 223 K.

Fig. 1.9 shows the mass chromatogram and MS spectra of the gaseous reaction product between CO_2 and F_2 in the presence of CsF. Fig. 1.9(a) shows that there were three peaks detected at the retention time of 9.04, 9.17, and 9.39 min. Peaks with m/z = 69 corresponding to CF_3^+ appeared in the MS spectra (Fig. 1.9(b) and (d)) at the retention time of 9.04 and 9.39 min. Ions with m/z = 47 and 66, corresponding, respectively, to COF^+ and COF_2^+, were observed at the retention time of 9.17 min. Especially, as shown in Fig. 1.9(d), the product had peaks with m/z = 151 and 170 corresponding to $C_2F_5O_2^+$ and $C_2F_6O_2^+$. Comparing the spectra to the data in the NIST Library, the products at 9.04, 9.17 and 9.39 min corresponded respectively to CF_4, COF_2 and CF_3OOCF_3.

Fig. 1.10 shows the reaction temperature dependence of the mass chromatogram of the reaction products in the presence of CsF. Two peaks at 8.96 and 8.99 min were detected in the profile, corresponding, respectively, to m/z = 47 and 66. The peak at 8.99 min disappeared at temperatures greater than 423 K. The MS spectrum for the product at 8.96 min was determined as COF_2. The two peaks in Fig. 1.10(a) proved that COF_2 was produced in two different pathways.

The GC / MS oven temperature was reduced to 224 K from 242 K to separate the two peaks. Fig. 1.11(a) shows a mass chromatogram of m/z = 47, 66 and 69. The two peaks in Fig. 1.10(a) were separated and two peaks with the fragment ion of m/z = 47 and 66 were apparent at the respective retention times of 9.16 and 9.23 min; the MS spectra of the two peaks also agreed with COF_2, as shown in Fig. 1.11(b)–2 and (b)–3. The intensity ratio of the two peaks was about 1 : 3. This peak intensity at the retention time of 9.23 min tended to decrease during storage of the sample. The peak disappeared completely after 18 days storage. It is inferred that $CF_2(OF)_2$ decomposed in the glass container to form SiF_4. It seems that one of two pathways of COF_2 formation must occur through the

process of the decomposition of $CF_2(OF)_2$ [14] in the GC column; the other pathway requires COF_2 to be produced in the reaction between CO_2 and F_2.

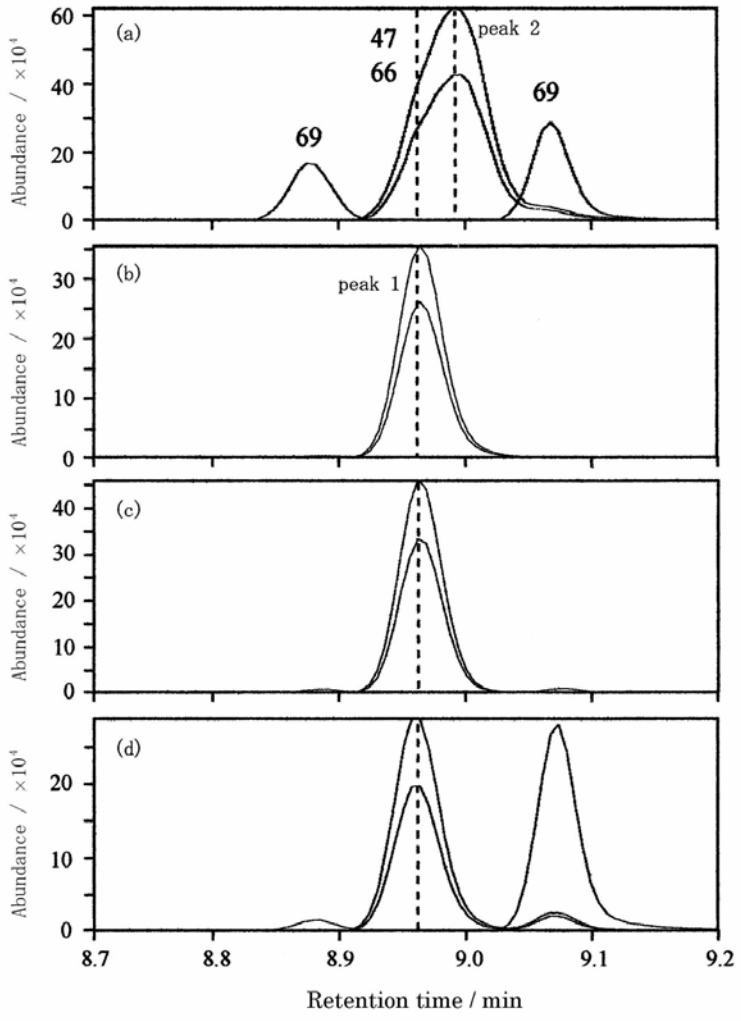

Fig. 1.10. Mass chromatograms of the products obtained in the presence of CsF at (a) 303 K, (b) 423 K, (c) 473 K and (d) 498 K. CO_2 : F_2 = 76 kPa : 76 kPa, reaction time 50 h, and GC oven temperature 243 K.

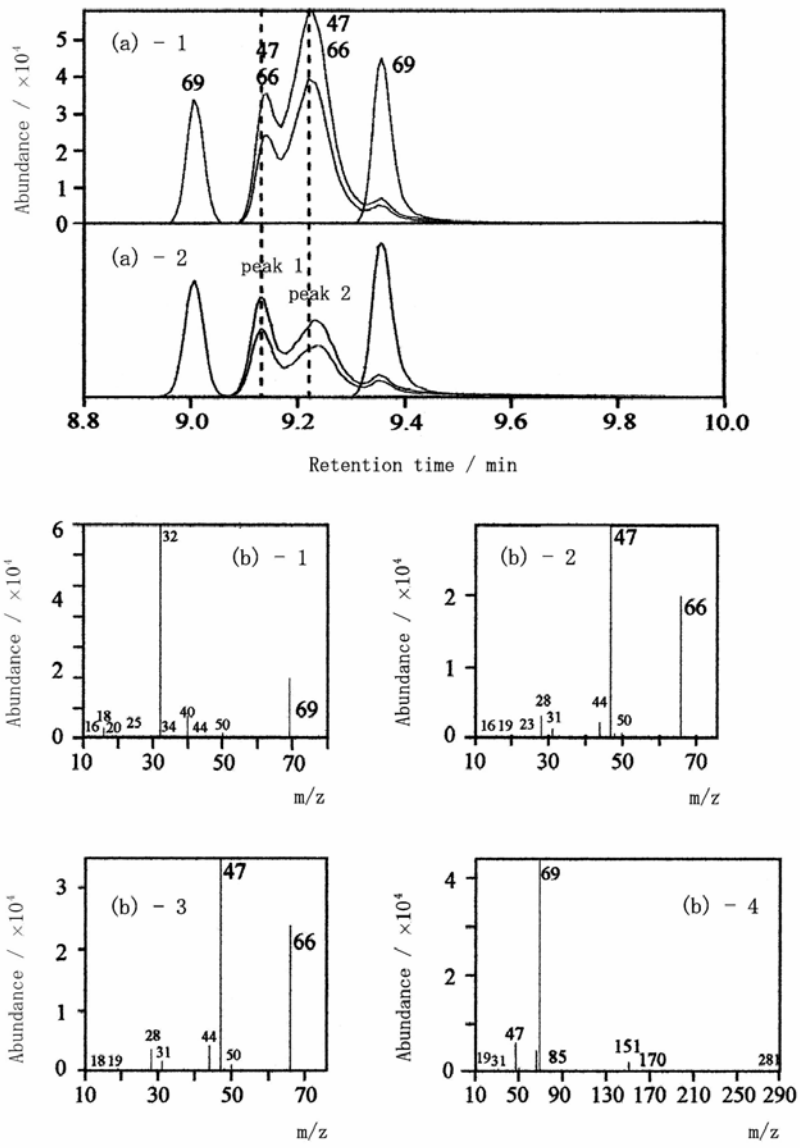

Fig. 1.11. Mass chromatogram of the products in the presence of CsF at the reaction temperature of 303 K. (a) Mass chromatograms at m/z = 69, 66 and 47 after (a)–1 0 and (a)–2 4 days. (b) Mass spectra of the sample in (a)–1 having the retention time of (b)–1 9.01 min, (b)–2 9.16 min, (b)–3 9.23 min and (b)–4 9.37 min. CO_2 : F_2 = 76 kPa : 76 kPa, reaction time 50 h, and GC oven temperature 223 K.

The product that had m/z = 69 at the retention time of ca. 9.37 min was also CF_3OOCF_3. The amount of CF_3OOCF_3 that was produced at 303 K was less than that at 498 K. Apparently, the formation of CF_3OOCF_3 of more than 498 K occurred under the low fluorine content condition. It was unrelated with the decomposition of $CF_2(OF)_2$ at 303 K. Formation of CF_4 did not proceed compared to the direct reaction.

The electronic states of metal fluorides before and after the reaction were analyzed using XPS. The color of EuF_3 and NaF changed from white to light yellow, whereas XPS profiles of the F 1s electron of EuF_3 and NaF did not change through the reaction. The color of CsF changed from white to pink in parts that contacted the nickel container. The color of CsF did not change in the parts that did not contact with the container. After a few days, the pink sample turned to yellow–green.

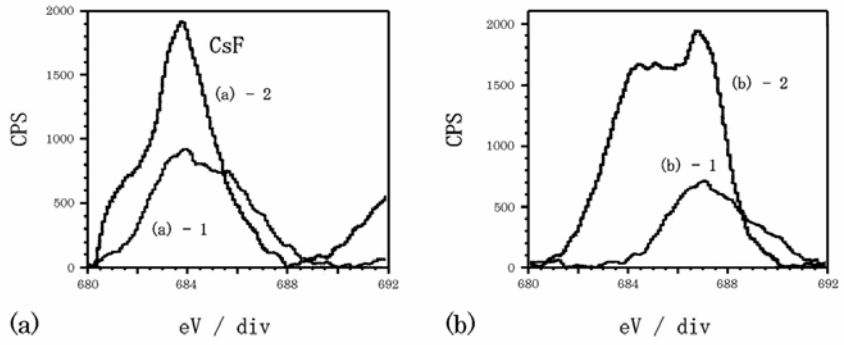

Fig. 1.12. XPS F1s spectrum of CsF before and after the reaction. (a) Before reaction: (a)–1 non–etching and (a)–2 after etching; (b) after reaction: (b)–1 non–etching and (b)–2 after etching.

Fig. 1.12 shows XPS spectra [25] of the F 1s electron in CsF before (a) and after (b) used as the catalyst. The peak at 683.9 eV appeared in the case of CsF before use. The peak at 685.6 eV is visible in Fig. 1.12(a). This peak must correspond to the F 1s electron of the organic compound adsorbed in CsF. This peak disappeared at 685.6 eV after 20 min of Ar ion etching, as shown in Fig. 1.12(a)–2. Therefore, it seems that the peak at 685.6 eV corresponded to some impurities on the surface of CsF. In Fig. 1.12(b), the peak at 687.1 eV appeared, no peak was detected at 684 eV before etching. The peak at 684.3 eV appeared after Ar ion etching, indicating that there must be two types of fluoride. The CsF surface was covered by some organic compound.

1.3.3. Yields

Quantitative analysis using the calibration line in Fig. 1.3 was carried out and the yield was calculated as a rate to CO_2. The yield of the whole gaseous reaction product after eliminating F_2 is shown in Table 1.3. In the direct reaction, yields of COF_2, CF_3OF, CF_4 and CF_3OOCF_3 increased with increasing reaction temperature and increasing reaction time, as shown in Fig. 1.13. The reaction rate under the condition of CO_2 / F_2 = 76 kPa / 76 kPa was smaller than that of CO_2 / F_2 = 50.7 kPa / 101.3 kPa. However, the yield of COF_2 of the reaction at CO_2 / F_2 = 76 kPa / 76 kPa was larger than that at CO_2 / F_2 = 50.7 kPa / 101.3 kPa.

Table 1.3

Yields of the products

Temperature (K)	Time (h)	Yield(%) COF_2	CF_3OF	CF_4	CF_3OOCF_3	$CF_2(OF)_2$
(a) Direct reaction						
CO_2/F_2 = 76kPa/76kPa						
303	5	0	0.7	0	0	0
373	5	0	0.7	0	0	0
373	50	0	0.8	0	0	0
423	5	0	1.4	0.1	0	0
423	50	0.8	8.5	0.1	0	0
473	5	0.5	10	0.1	0	0
473	49	2.6	17	0.5	0	0
498	2	0.2	3.5	0.2	0	0
498	5	0.8	8	0.3	0	0
498	10	0.4	6.6	0.1	0	0
498	20	1.3	9.5	0.6	0	0
498	30	1.3	13.8	0.3	0	0
498	40	2.5	16.4	0.7	0	0
498	50	2.2	20	1.1	0	0
498	60	4.5	19.1	1.9	0	0
498	72	11.1	32.1	4.6	0	0
525	50	3.4	26.7	2.6	0	0
CO_2/F_2 = 50.7kPa/101.3kPa						
498	2					
498	5					
498	10					
498	20	2.4	30.8	0.8	0	0
498	30					
498	40					
498	50	6	51.5	1.5	0	0
498	60	4.3	45.2	1.9	0	0
498	72	5.3	43.4	1.8	0	0
(b) In the presence of CsF(3g)						
CO_2/F_2 = 76kPa/76kPa						
303	5	0.3	0	0	0.1	19.5
303	50	0.5	0	0	0.1	36.4
373	5					
373	50	3.4	12.9	0	0	11.4
423	5					
423	50	4.4	22.3	0	0	5.6
473	5					
473	50	6.5	23.3	0.1	0.1	0
498	2					
498	5	3.7	11.1	0	0.4	0
498	10					
498	20	2.5	27.4	0	0.2	0
498	30					
498	40					
498	50	2.9	17.2	0.2	2.5	0
498	60					
498	72					

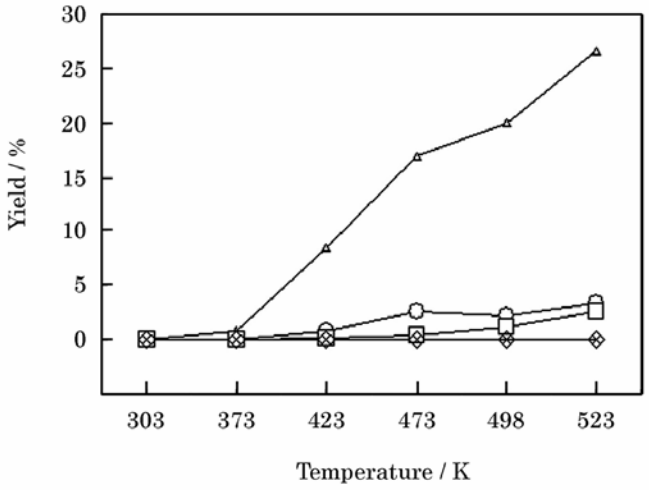

Fig. 1.13. Yields of products in the direct reactions at various temperatures. CO_2 : F_2 = 76 kPa : 76 kPa and reaction time 50 h. (○) CF_2O, (△) CF_3OF, (□) CF_4, (◇) CF_3OOCF_3 and (×) $CF_2(OF)_2$.

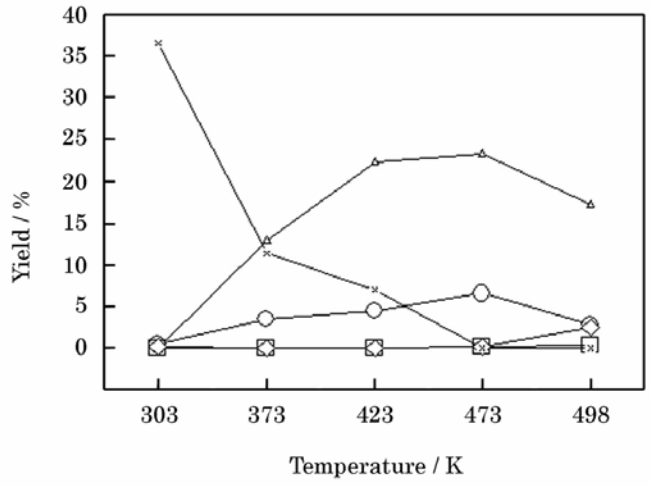

Fig. 1.14. Yields of products in the presence of CsF at various temperatures. CO_2 : F_2 = 76 kPa : 76 kPa and reaction time 50 h. (○) CF_2O, (△) CF_3OF, (□) CF_4, (◇) CF_3OOCF_3 and (×) $CF_2(OF)_2$.

In the presence of CsF (3 g), the yields of COF_2, CF_3OF, CF_4, CF_3OOCF_3 and $CF_2(OF)_2$ were measured under the conditions of CO_2 / F_2 = 76 kPa / 76 kPa, with 50 h reaction time. The yields, which are shown in Fig. 1.14, did not increase monotonously with increasing reaction temperature. The yield of $CF_2(OF)_2$ decreased with increasing temperature. The yields of COF_2 and CF_3OF had the highest values. In addition, CF_3OOCF_3 was detectable at temperatures higher than 498 K. The yields of COF_2 and CF_3OF become larger in the presence of CsF than in the direct reaction at temperatures of 373–473 K. Furthermore, the yields of CF_3OOCF_3 appeared at the high–temperature range over 473 K. However, CF_4 was only slightly observed in the presence of CsF, as shown in Fig. 1.14. Total yields of the reaction products were equal, about 23%, for both reactions at 498 K.

On the other hand, in the presence of 0.25 g (1.65×10^{-3} mol) CsF, the reaction product was similar to the direct reaction. The different yields of COF_2 and CF_3OF can be explained using the reaction mechanism.

In the presence of 0.35 g (1.65×10^{-3} mol) EuF_3 under the condition of CO_2 / F_2 = 76 kPa / 76 kPa at the reaction time of 50 h, the yields of COF_2, CF_3OF, CF_4 and CF_3OOCF_3 are shown in Fig. 1.15. Those yields were identical to those of the direct reaction. It appears that the amount of EuF_3 was insufficient to hasten the reaction.

Fig. 1.16 shows the yield of the direct reaction under the condition of CO_2 / F_2 = 76 kPa / 76 kPa at 498 K. In this case, it seemed that the yields of COF_2, CF_3OF and CF_4 at the direct reaction increased with increasing reaction time, as shown in Table 1.3.

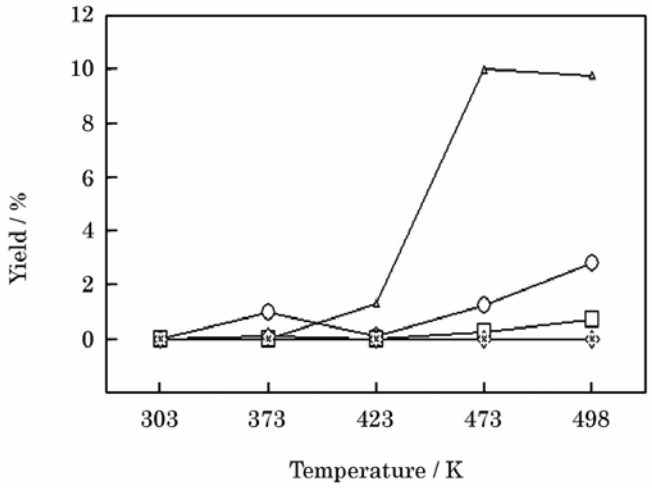

Fig. 1.15. Yields of products in the presence of EuF_3 at various temperatures. CO_2 : F_2 = 76 kPa : 76 kPa and reaction time 50 h. (○) CF_2O, (△) CF_3OF, (□) CF_4, (◇) CF_3OOCF_3 and (×) $CF_2(OF)_2$.

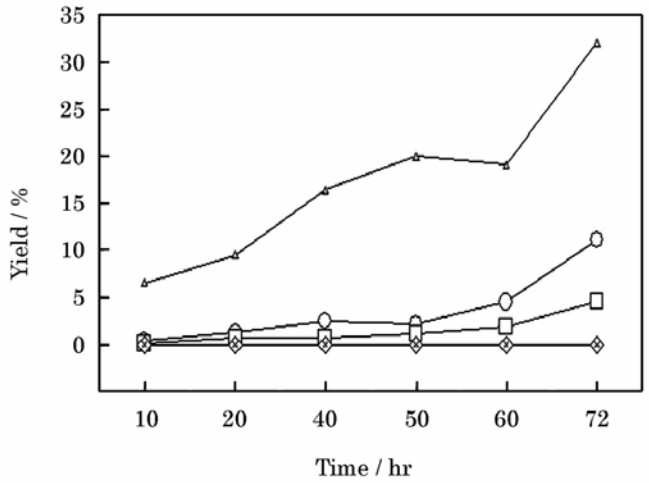

Fig. 1.16. Yields of products in the direct reaction at 498 K with various reaction times. CO_2 : F_2 = 76 kPa : 76 kPa. (○) CF_2O, (△) CF_3OF, (□) CF_4, (◇) CF_3OOCF_3 and (×) $CF_2(OF)_2$.

In summary, the best yield of COF_2 was 11.1% under the reaction condition of CO_2 / F_2 = 76 kPa / 76 kPa, with reaction temperature of 498 K and reaction time of 72 h. In the presence of CsF, the best yield of COF_2 was 6.5% under the reaction conditions of CO_2 / F_2 = 76 kPa / 76 kPa, with reaction temperature of 473 K and reaction time of 50 h.

1.3.4. Reaction rate

The reaction of COF_2 generation can be written as $CO_2 + F_2 = COF_2$. For the reaction rate, ν is $k[CO_2][F_2]$, where k is a rate constant.

The whole amount of COF_2 produced during the reaction process was calculated as the amount of the products that were produced through COF_2 pathways such as COF_2, CF_3OF, CF_4 and CF_3OOCF_3 in the direct reaction. However, under the existence of CsF (3 g) it was calculated as the total of COF_2, CF_4 and CF_3OOCF_3.

Table 1.4

Formation rate of COF_2 and rate constant and activation energy of COF_2 formation

Catalyst	Pressure (kPa)		Temperature,	Formation rate,	Rate constant,	Activation energy
	CO_2	F_2	T (K)	v (mol dm^{-3} h^{-1})	k (dm^{-3} mol^{-1} h^{-1})	(kJ mol^{-1})
none	50.7	101.3	498	2×10^{-4}	1.63	
	76	76	373	0.4×10^{-5}	0.00594	45.7
	76	76	423	0.5×10^{-4}	0.0859	
	76	76	473	1×10^{-4}	0.208	
	76	76	498	1×10^{-4}	0.232	
CsF (3g)	76	76	303	6×10^{-6}	0.00966	24.2
	76	76	373	2×10^{-5}	0.0402	
	76	76	498	5×10^{-4}	1.88	
EuF_3 (0.35g)	76	76	373	0.5×10^{-5}	0.00629	38.9
	76	76	423	0.8×10^{-5}	0.00932	
	76	76	473	0.6×10^{-4}	0.0789	
	76	76	498	0.8×10^{-4}	0.121	

The COF_2 formation rates and rate constants are shown in Table 1.4. The COF_2 formation rates in the presence of CsF were five times larger than those without any catalyst.

1.3.5. Activation energy of COF_2 formation

The activation energy of COF_2 is estimated according to the following reaction. The relation between the rate constant k and the temperature T is usually expressed as an Arrhenius reaction:

$$k = A\,e^{-E/RT}$$

The value of the activation energy E was determined from the gradient of the plots of $\ln k$ vs $-1/T$.

The values of the activation energy are shown in Table 1.4. The activation energy in case of using CsF was the smallest among all that were obtained.

1.3.6. Reaction mechanism

Any halogen, X_2, may react by either of two mechanisms as the following.

(i) atomic, often light– and heat–catalyzed, leads to the active $X^{\bullet}$.

(ii) ionic, leads to the active X^{-}.

However, fluorine [7, 8] is the most electronegative of all elements, and has a high positive nuclear charge, it should react atomically rather than ionically. Because the complete removal of electron from it, to form a positive F^{+} ion, would be very difficult.

The gas phase fluorinations by direct reaction with fluorine as well as in the metal

fluoride are known for a wide variety of reactions.

The following reaction mechanisms are reasonable to explain the observed products.

The radical reaction probably takes place, especially in the gas phase between CO_2 and F_2. The reaction mechanism will be considered as the following:

$$F_2 \xrightarrow{\triangle} F^{\bullet} \quad (1)$$

$$CO_2 + F^{\bullet} \rightarrow CF(O)O^{\bullet} \quad (2)$$

$$CF(O)O^{\bullet} + F_2 \rightarrow COF_2 + OF^{\bullet} \quad (3)$$

$$OF^{\bullet} + F_2 \rightarrow OF_2 + F^{\bullet} \quad (4)$$

$$COF_2 + F^{\bullet} \rightarrow CF_3O^{\bullet} \quad (5)$$

$$CF_3O^{\bullet} + F_2 \rightarrow CF_3OF + F^{\bullet} \quad (6)$$

$$CF_3OF + F^{\bullet} \rightarrow CF_3^{\bullet} + OF_2 \quad (7)$$

$$CF_3^{\bullet} + F_2 \rightarrow CF_4 + F^{\bullet} \quad (8)$$

$$CF_3O^{\bullet} + CF_3O^{\bullet} \rightarrow CF_3OOCF_3 \quad (9)$$

$$CF_3O^{\bullet} + CF_3O^{\bullet} \rightarrow CF_3OF + COF_2 \quad (10)$$

$$OF^{\bullet} + OF^{\bullet} \rightarrow F_2 + O_2 \quad (11)$$

The fluorine radical ($F^{\bullet}$) is produced by the dissociation of F_2 in reaction (1); subsequently, $F^{\bullet}$ might go on to react with CO_2. In this case, the $F^{\bullet}$ formation is hastened by heating in the initiation step (reaction (1)). The reaction (1) proceeds very slowly at room temperature; it proceeds remarkably faster at 473 K.

Some subsequent steps are shown in reactions (2)–(8), and COF_2, CF_3OF and CF_4 are produced. These products were detected as described above. Many other subsequent steps are possible; they might proceed in parallel.

Similarly, the termination steps are shown in reactions (9)–(11), and CF_3OF and

CF_3OOCF_3 are produced. Thus, this direct reaction process, including the reactions (1)–(11), involves a free radical chain reaction [26]. In our present experiment, it seemed that reaction (9) proceeded only slightly.

On the other hand, another reaction between CO_2 and F_2 can occur. Hohorst and Shreeve report that when the reaction temperature is near room temperature and the F_2 amount is sufficient under the existence of CsF, the reaction product between CO_2 and F_2 is $CF_2(OF)_2$ [24]. However, CF_3OF and OF_2 are formed when the reaction temperature rises and the F_2 amount is insufficient. Identical results were confirmed through our experiments.

In the first step, the adsorption of F_2 on the CsF surface must take place. The first ionization energy of Cs is 3.89 eV. In addition, fluorine has the largest electronegativity. Therefore, CsF is the material that has the highest ionic bond. This highly ionic bond apparently causes the larger polarization of F_2 molecule adsorbed on CsF. This polarization of the F_2 molecule might promote the reaction between CO_2 and F_2.

It has also been reported that atomic fluorine [27] must be generated easily at the CsF interface. The atomic fluorine might proceed to react with CO_2 as well as fluorine radical.

$$F_2 \xrightarrow{CsF} 2\,F$$

In many reactions, the reaction intermediates should be postulated. The XPS analyses of the CsF surface give some information about the organic compounds as intermediates.

In the second step, it seems to form $CF_2(OF)_2$ by passing through reactions (12)–(14). The possible reaction intermediates of $[CF(O)O^{\delta-}Cs^{\delta+}F]$ and $[CF_2(OF)O^{\delta-}Cs^{\delta+}F]$

[28–30] shown in the following reactions must be formed:

$$CO_2 + F_2 + CsF \rightarrow [CF(O)O^{\delta-}Cs^{\delta+}F],\ CsF(CF(O)OF) \quad (12)$$

$$[CF(O)O^{\delta-}Cs^{\delta+}F] + F_2 \rightarrow [CF_2(OF)O^{\delta-}Cs^{\delta+}F] \quad (13)$$

$$[CF_2(OF)O^{\delta-}Cs^{\delta+}F] + F_2 \rightarrow CF_2(OF)_2 + CsF \quad (14)$$

At temperatures higher than 303 K or under low fluorine gas pressure, CF_3OF seems to form, leaving OF_2 by reaction (15) instead of proceeding to reaction (14):

$$[CF_2(OF)O^{\delta-}Cs^{\delta+}F] + CsF \rightarrow CF_3OF + OF_2 + Cs_2O \quad (15)$$

$$Cs_2O + F_2 \rightarrow CsF + OF_2 \quad (16)$$

The concentration of F_2 adsorbed on the surface must decrease with increasing temperature. Therefore, it seems to be difficult for the intermediate compound to react with the F_2 molecule. The possible reaction intermediate $[CF_2(OF)O^{\delta-}Cs^{\delta+}F]$ reacts with CsF, and CF_3OF must be formed by reactions (15) and (21). In fact, Cs_2O reacts immediately with F_2, as in reaction (16), and it will return to CsF. The low F_2 concentration on the CsF surface induced by the low F_2 pressure yields the similar result to that shown above.

Fig. 1.14 shows the temperature dependence of the yield of COF_2. It seems that pathways (17)–(21) are considered to form COF_2 and CF_3OF [31–33]. With rising temperature, OF_2 would be similarly produced as follows; OF_2 would remain in the products at higher temperature like in case of CF_3OF:

$$[CF(O)O^{\delta-}Cs^{\delta+}F] + F_2 \rightarrow COF_2 + OF_2 + CsF \quad (17)$$

$$[CF(O)O^{\delta-}Cs^{\delta+}F] + CsF \rightarrow COF_2 + Cs_2O \quad (18)$$

$$[CF_2(OF)O^{\delta-}Cs^{\delta+}F] + F_2 \rightarrow COF_2 + OF_2 + CsF \quad (19)$$

$$CF_2O + CsF \rightarrow [CF_3O^{\delta-}Cs^{\delta+}F] \quad (20)$$

$$[CF_3O^{\delta-}Cs^{\delta+}F] + F_2 \rightarrow CF_3OF + CsF \quad (21)$$

Fig. 1.14 shows that the yield of CF_3OF increased with rising reaction temperature in the temperature range of 373–473 K. The formation and stability of the possible intermediates such as $[CF(O)O^{\delta-}Cs^{\delta+}F]$, $[CF_2(OF)O^{\delta-}Cs^{\delta+}F]$ and $[CF_3O^{\delta-}Cs^{\delta+}F]$ must be examined to explain the change in CF_3OF yield. This situation will be estimated from XPS analysis of the CsF used for the reaction. The binding energy of the F 1s electron on the CsF surface was analyzed using XPS (Fig. 1.12). After the reaction, the XPS profile of F 1s electron shows a peak at 687.1 eV that corresponds to the C–F bond. The XPS profile after etching has a peak at 684.3 eV that corresponds to CsF. Results showed that the organic compounds including C–F bond were adsorbed onto the CsF surface. These organic compounds must be intermediates.

On the other hand, it is considered that the radical [34] reaction must contribute to the increased CF_3OF yield at temperatures of 373–473 K. However, comparing Fig. 1.13 with Fig. 1.14 at 498 K, the radical reaction must only slightly contribute to the increase of the CF_3OF yield. Fig. 1.14 shows that the yields of COF_2 and CF_3OF decreased over 473 K. That is, they have a maximum value around 474 K. With the change of the reaction temperature, it seems that the kinds of the reaction intermediates change on the CsF surface. At low temperatures, the possible reaction intermediates of $[CF(O)O^{\delta-}Cs^{\delta+}F]$ and $[CF_2(OF)O^{\delta-}Cs^{\delta+}F]$ must be formed by reactions (12)–(14); $CF_2(OF)_2$ is formed dominantly at room temperature. The COF_2 and CF_3OF must be formed dominantly from the reaction intermediates by reactions (15)–(21) at temperatures of 373–473 K. The formation of CF_3OF becomes dominant. At temperatures greater than 498 K, the reaction through the possible intermediate $[CF_3O^{\delta-}Cs^{\delta+}F]$ will become

dominant. Furthermore, some reactions exist in which the possible reaction intermediates of $[CF(O)O^{\delta-}Cs^{\delta+}F]$, $[CF_2(OF)O^{\delta-}Cs^{\delta+}F]$ and $[CF_3O^{\delta-}Cs^{\delta+}F]$ might undergo competing reactions to give different products such as COF_2, CF_3OF, CF_4 and CF_3OOCF_3.

CF_3OOCF_3 is formed by the following reaction:

$$2\,[CF_3O^{\delta-}Cs^{\delta+}F] \rightarrow CF_3OOCF_3 + CsF \qquad (22)$$

As inferred from the results shown in Fig. 1.14, reaction (22) must take place significantly at temperatures greater than 473 K. Yields of CF_3OF might decrease because of the consumption of $[CF_3O^{\delta-}Cs^{\delta+}F]$ by reaction (22). Table 1 shows that CF_3OOCF_3 was also produced at 303 K in 0.1%. This fact can not be explained using the reaction scheme described above. There is probably a reaction path way through which CF_3OOCF_3 is produced from $CF_2(OF)_2$, which is the major product at 303 K.

The formation of CF_4 described by reaction (23) scarcely occurred, as shown in Fig. 1.14:

$$[CF_3O^{\delta-}Cs^{\delta+}F] + F_2 \rightarrow CF_4 + O_2 + CsF \qquad (23)$$

As described above, it became the possible major intermediate instead of $[CF_2(OF)O^{\delta-}Cs^{\delta+}F]$ at temperatures greater than 473 K. It is easily converted to CF_3OF and CF_3OOCF_3 because $[CF_3O^{\delta-}Cs^{\delta+}F]$ must react with F_2 to generate CF_4. The reactions (21) and (22) proceed rapidly more than reaction (23), thereby giving low CF_4 yield.

The competitive reaction processes mentioned here are summarized in scheme 2.

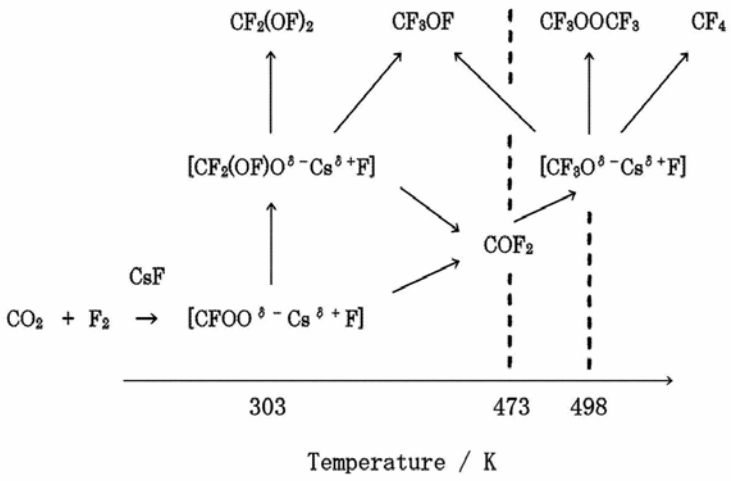

Scheme 2. Scheme of competitive reaction processes. Blanketed compounds are the possible intermediates.

References and notes

[1] J. C. Amphlett, J. R. Dacey, G. O. Pritchard, J. Phys. Chem. 75 (1971) 3024–3026.

[2] G. H. Cady, Inorg. Synth. 8 (1966) 165–170.

[3] Kwasnik in handbook of Preparative Inorganic Chemistry, Vol.1, G. Brauer, Ed. (Academic Press Inc., New York, 2th ed., (1963) pp. 206–208.

[4] F. A. Hohorst, J. M. Shreeve, J. Am. Chem. Soc. 89 (1966) 1809–1810.

[5] R. L. Cauble, G. H. Cady, J. Am. Chem. Soc. 89 (1967) 1962.

[6] R. L. Cauble, G. H. Cady, J. Am. Chem. Soc. 89 (1967) 5161–5162.

[7] P. Politzer, J. Am. Chem. Soc. 91 (1969) 6235–6237.

[8] The Entrance of Fluorine Chemistry, 155 Committee of Fluorine Chemistry. (Printed in Japan, 1999)

[9] Satoshi Ueda, Yasuo Hasegawa, Susumu Yonezawa, Masayuki Takashima, International Chemical Congress of Pacific Basin Societies, Honolulu, Hawaii, December, 2000, Book of Abstracts, P. 1487.

[10] R. Otani, S. Yonezawa, M. Takashima, Master Dissertation (2002).

[11] Yasuo Hasegawa, Reiko Otani, Susumu Yonezawa, Masayuki Takashima, J. Fluorine Chem. 128 (2007) 17–28.

[12] Gregor Hoogers, Fuel Cell Technology Handbook (CRC press, 2003).

[13] W. M. Latimer, The Oxidation States of the Elements and Their Potentials in Aqueous Solutions (Prentice Hall, New York, 1952).

[14] P. G. Thompson, J. Am. Chem. Soc. 89 (1966) 1811–1813.

[15] A. J. Arvia, P. J. Aymonino, Spectrochim. Acta 18 (1962) 1299–1309.

[16] R. S. Porter, G. H. Cady, J. Am. Chem. Soc. 79 (1957) 5628–5631.

[17] A. H. Nielsen, T. G. Burke, P. J. H. Woltz, E. A. Jones, J. Chem. Phys. 20 (1952) 596–604.

[18] Private communication with Central Glass Co. Ltd. for COF_2: FT–IR(CaF_2): cm^{-1},(T%): 1957vs(32%), 1943vs(25%), 1929vs(23%), 1256vs(24%), 1231vs(23%), 977s(70%) and 959s(70%).

[19] R. T. Legemann, E. A. Jones, P. J. Woltz, J. Chem. Phys. 20 (1952) 1768–1771.

[20] Selected data for CF_4: FT–IR(CaF_2, cm^{-1}): 1280vs; EI–MS: m/z(%): 69(CF_3^+,100), 50(CF_2^+,10); CI–MS: m/z(%): 69($[M-19]^+$,100), 89($M+H^+$,6).

[21] Selected data for COF_2: FT–IR(CaF_2, cm^{-1}): 1957vs, 1943vs, 1929vs, 1256vs, 1231vs, 977s and 959s; EI–MS: m/z(%): 47(COF^+,100), 66(COF_2^+,60); CI–MS: 67($M+H^+$,100), 47($[M-19]^+$,25).

[22] L. R. Anderson, W. B. Fox, J. Am. Chem. Soc. 89 (1967) 4313–4315.

[23] J. M. Huston, M. H. Studier, J. Fluorine Chem. 13 (1979) 235–249.

[24] F. A. Hohorst, J. M. Shreeve, Inorg. Synth. 11 (1968) 143–147.

[25] NIST XPS Database (2003).

[26] G. Chiltz, P. Goldfinger, G. Huybrechets, G. Martens, G. Verbeke, Chem. Rev. 63 (1963) 355–372.

[27] G. H. Cady, Anales Asoc. Quim. Argentina 59 (1959) 618.

[28] B. S. Ault, Inorg. Chem. 21 (1982) 756–759.

[29] L. R. Anderson, W. B. Fox, Inorg. Chem. 9 (1970) 2182–2183.

[30] L. Lawlor, J. Passmore, Inorg. Chem. 18 (1979) 2923–2924.

[31] M. Wechsberg, G. H. Cady, J. Am. Chem. Soc. 91 (1969) 4432–4436.

[32] M. E. Redwood, C. J. Willis, Can. J. Chem. 43 (1965) 1893–1898.

[33] M. Lusting, A. R. Pitochelli, J. K. Ruff, J. Am. Chem. Soc. 89 (1967) 2841–2843.

[34] R. F. Merritt, J. Org. Chem. 32 (1967) 4124–4126.

Chapter 2

Preparation of COF_2 using CO_2 and F_2 in the electrochemical cell with $PbSnF_4$ as a solid electrolyte

2.1 Introduction

On the earth each year, 12,100 million tonnes of CO_2 are emitted to the air [1]. The increase of its concentration in the air is causing global warming. Numerous efforts have been made to remove CO_2 from the air. Normally, new methods to reduce CO_2 to CH_3OH and CH_4 have been investigated [2–3]. These investigations are based on the concept that CO_2 is a final product of hydrocarbon compounds' combustion.

A strong oxidant, F_2, can oxidize the oxides. Previously, we reported a reaction between CO_2 and F_2 to form COF_2 [4]. By this reaction, CO_2 can be converted to COF_2. The Gibbs free energy change of this reaction is calculated as 220 kJ mol^{-1} [5].

$$CO_2 + F_2 \rightarrow COF_2 + 1/2\ O_2 + (-\Delta G)\ 220\ kJ\ mol^{-1}$$

Furthermore, the theoretical electromotive force calculated from its Gibbs free energy is 1.14 V, which value is mostly equal to the electromotive force 1.23 V of the H_2 / O_2 fuel cell [6]. Based on this idea, we tried to investigate COF_2 formation using CO_2 and F_2 in the electrochemical cell with $PbSnF_4$.

By using the electrochemical cell with solid electrolyte to prepare COF_2, the reaction between CO_2 and F_2 might be controlled by external current flow and the separation of COF_2 from CO_2 / F_2 mixture gas is not needed.

Tetragonal $PbSnF_4$ [7–22] is known as a fluoride ion conductor having high electric conductivity at ambient temperatures. $PbSnF_4$ can exist in several polymorphic forms as described by many reports [7, 8, 14–16], and has a very complex system of phase transitions.

The CO_2 / F_2 electrochemical cell was constructed using tetragonal $PbSnF_4$ as a solid electrolyte and its performance was investigated in detail.

2.1.1 What is a CO_2 / F_2 electrochemical cell?

The electrochemical cell potential is a measure of the maximum amount of energy per unit charge which is available to do work. This maximum work is equal to the change in Gibbs free energy, ΔG in the reaction. The ideal performance of a cell is defined by its Nernst potential [23], E°, or the ideal cell voltage. The maximum potential difference is called the electromotive force (emf), E_{emf}. The general Nernst equation correlates the Gibbs free energy ΔG.

For reactions, the net free energy change is directly related to the voltage, and the relationship between free energy change ΔG and the cell voltage E can be expressed as

$$\text{Maximum work} = \Delta G = -nF\Delta E$$

$$\Delta E = \Delta E^{\circ} - (RT/nF)\,\text{In}([\text{Red}] / [\text{Ox}])$$

where F is the Faraday's constant, n is the number of electrons transferred in the half–reaction, [Red] is the concentration of the reduced species, and [Ox] is the

concentration of the oxidized species.

As described above, CO_2 can be converted to COF_2. Therefore, the theoretical electromotive force calculated from its Gibbs free energy is 1.14 V.

Because of the large reactivity of F_2 to H_2O, solid electrolytes [24] are needed. A large number of solid–state materials that exhibit ionic conductivity are known today, and many efforts have been made to understand the ion conduction mechanism at the molecular level. Recently, many fluoride ion conductors have been reported, and $PbSnF_4$ has been used for the design of chemical sensors [20].

2.1.2 Electrochemical impedance spectroscopy

To investigate the electrochemical properties of tetragonal $PbSnF_4$, ac impedance spectroscopy is a convenient technique.

The electrochemical reaction at the electrode–electrolyte interface cannot be fully understood using traditional electrochemical measurements. A complete description requires impedance measurement made over a broad frequency range at various potentials and determination of all the electrical characteristics of the interface, which can be though of as a thin capacitor that forms between the charged electrode and the counter ions lined up parallel to it [25, 26].

An interface is described by an equivalent circuit. The electrochemical reaction rates are better understood using electrochemical impedance spectroscopy. Scheme 3 shows some components of impedance such as Rb, Rg and Re.

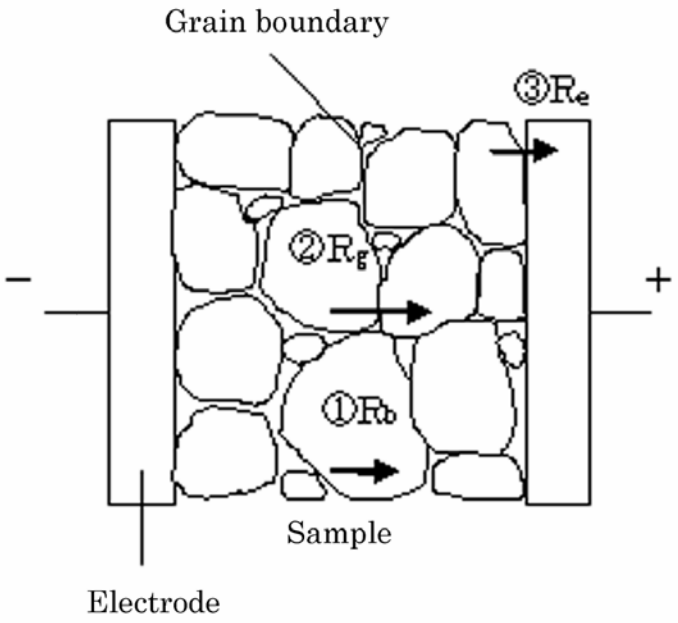

Scheme 3. Some components of electrochemical impedance measurement for solid electrolyte.

In a simple case, the interface can be modeled by an equivalent circuit as shown in Fig. 2.1, also called a Randles circuit [27–29], made of a double–layer [30] capacitor in parallel with a polarization resistor (also known as a charge transfer resistor) and a Warburg impedance.

Impedance is a totally complex resistance encountered when a current flows through a circuit made of resisters, capacitors, or inductors, or any combination of these. The impedance of the interface consists of two parts, a real number *Z'* and an imaginary number *Z"* with a complex representation.

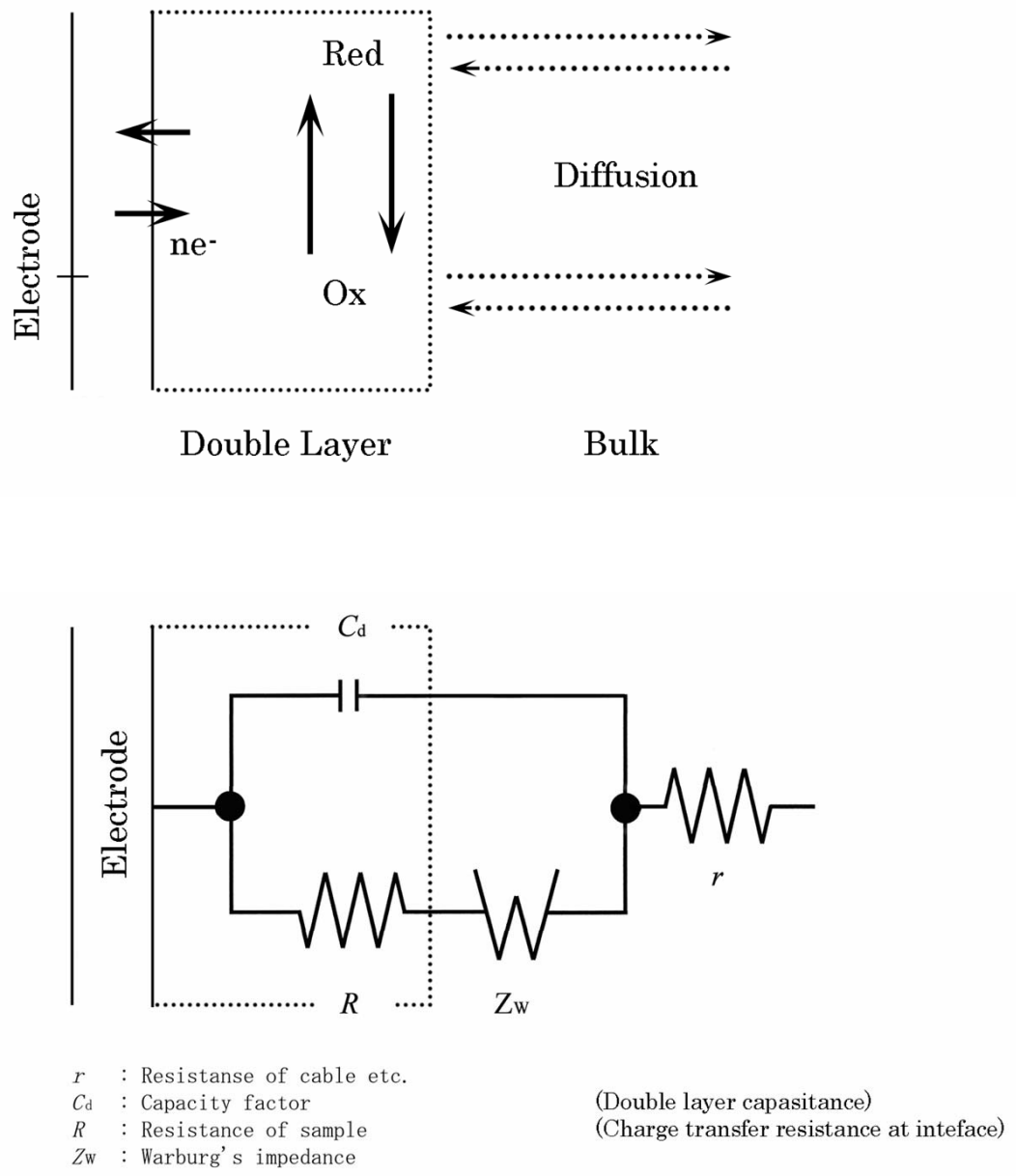

Fig. 2.1. Randles equivalent circuit and electric components.

Extraction of the system characteristics requires interpreting the Cole–Cole plot (Fig. 2.2) according to following equation.

$$Z(\omega) = r + R / (1 + j\omega RC_d) =$$

$$r + R / (1 + \omega^2 R^2 C_d^2) - j\omega R^2 C_d / (1 + \omega^2 R^2 C_d^2) = Z' + jZ''$$

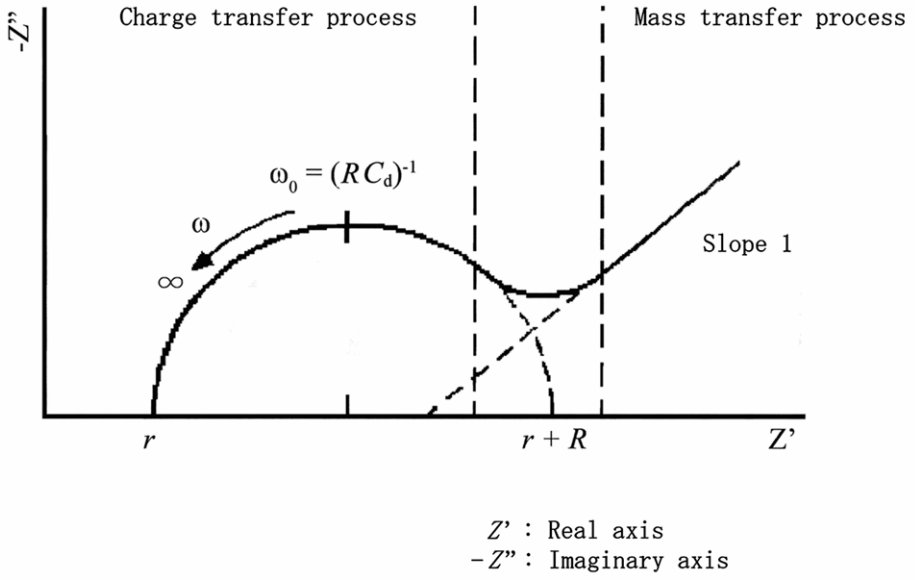

Fig. 2.2. Cole–Cole plot for Randles equivalent circuit.

According to the simulated equivalent circuit, the real and imaginary components of the impedance can be calculated as $Z' = r + R / (1 + \omega^2 R^2 C_d^2)$ and $Z'' = \omega R^2 C_d / (1 + \omega^2 R^2 C_d^2)$, respectively [31].

At high frequencies, the frequency dependent term, $\omega = 2\pi f$, is high and $\omega^2 R^2 C_d^2 \gg 1$, then, $Z(\omega) = Z'(\omega) = r$, $Z''(\omega) = 1 / \omega C_d \fallingdotseq 0$, which is an intercept on the Z' axis on the high–frequency side. For $\omega \fallingdotseq 0$, $Z(\omega) = r + R$, which is an intercept on the Z' axis on the low–frequency side.

This technique will offer the most powerful analysis on the status of electrodes during charging–discharging processes of batteries and electrochemical cells as well as

corrosion experiments. More importantly, this technique may be used to monitor and prove many different processes that occur during electrochemical experiments, including adsorption of reactants and products as well as various reactions that either precede or follow the experiments, thereby changing the electrical characteristics of electrode–electrolyte interfaces.

In an ideal electrochemical cell, the ionic current through the electrolyte ($PbSnF_4$) inside the cell matches an electronic current through an external load. A solid electrolyte acts as a separator of two electrodes as well as a carrier of the internal ionic current. It is in the form of an electrolyte of thickness L and area A (cross–sectional area) that separates electrically the two electrodes of the cell. The electrical conductivity (σ_i) can be calculated by following equation.

$$\sigma_i = L / (R \times A)$$

where σ_i is the ionic conductivity of the electrolyte. For a current i through the cell, the voltage $i \cdot R$ represents a potential drop [8].

The frequency response analyzer (Fig. 2.3) has become the industry standard in electrochemical instrumentation in recent years. The reference ac wave of frequency ω superimposed on a given dc bias potential is applied to a working electrode in the electrical cell.

The entire frequency range must be scanned by generating ac voltage wave of 10–20 representative frequencies per decade to make measurements. Often, measurements of more than a few ac cycles are necessary at a given frequency to obtain a decent S/N, and the instrument usually wait for the system to reach a constant current after a step to a desired dc bias potential before it takes measurements.

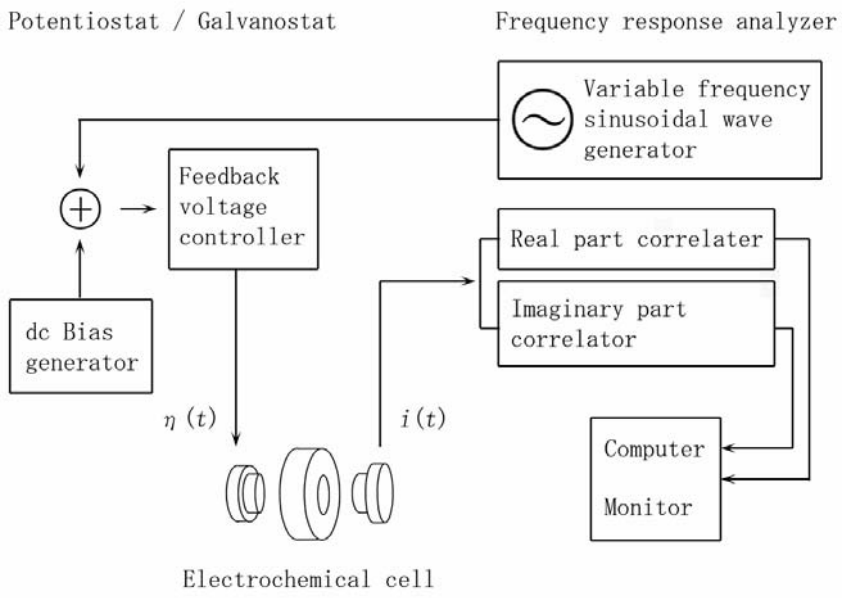

Fig. 2.3. Concept of the frequency response analyzer.

2.2 Experimental

2.2.1 Preparation of $PbSnF_4$

$PbSnF_4$ was prepared by adding a 1.01 M aqueous solution of $Pb(NO_3)_2$ (99.5%) to a freshly prepared 2.47 M aqueous solution of SnF_2 (99%) with the ratio of Pb / Sn = 0.25:

$$Pb(NO_3)_2 + 4\ SnF_2 \rightarrow PbSnF_4 + Sn(NO_3)_2 + 2\ SnF_2$$

The white sediment prepared by dropping $Pb(NO_3)_2$ aqueous solution to SnF_2 aqueous solution was suction–filtered and placed in vacuum (ca. 10^{-2} mm of Hg) for at least 4 h.

Table 2.1

Parameters for preparing $PbSnF_4$ in this study

Parametr	Description	Range
	$Pb(NO_3)_2$ / SnF_2 molar ratio in the reaction mixture	0.25
Time($PbSnF_4$)	time between the end of the addition of $Pb(NO_3)_2$ and the filtration of the product	0 hour
C(SnF_2)	concentration of SnF_2	2.47 M
C($Pb(NO_3)_2$)	concentration of $Pb(NO_3)_2$	1.01 M
Gas	atmosphere over the reaction	air
Rate	rate of addition of one solution into the other	0.5 mL / min
Order	$Pb(NO_3)_2$ solution is added to the SnF_2 solution	Pb in Sn
Temerature	temperature of the reaction	Room Temp.

2.2.2 Characterization of $PbSnF_4$

The sample was characterized using X–ray diffraction (XRD) and analyzed by energy dispersive X–ray fluorescence spectrometry (XFS), density measurement, and quantitative analysis of fluoride ion.

Using XFS (EDX–800; Shimadzu Corp.), a calibration curve was plotted for quantitative analysis of samples. The molar ratios of PbF_2 and SnF_2 in pellets as standard samples were adjusted to 1 : 0, 1 : 4, 2 : 3, 3 : 2, 4 : 1, and 0 : 1. Density was measured (Micrometics Accupyc 1330; Shimadzu Corp.).

A fluoride–ion–selective electrode (SA720; Orion Research Inc.) and ion chromatography (Tosoh Corp.) were used for quantitative analyses of fluoride ions.

The spacing of atoms in a solid can be measured using X–rays. X–ray diffraction data were collected using a diffractometer (XD–3As; Shimadzu Corp.) with Cu Kα radiation (1.5418 Å). Data were collected at a scan rate of 2 ° / min by sampling pitch 0.034 °, with

a preset time of 4 s. Rietveld analyses of the X–ray power diffraction pattern were carried out. The crystal structure parameters were refined using Rietveld analysis with the RIETAN–2000 program [32].

The sample of about 1 g was compacted into a pelleter. After vacuuming for 15 min, the sample was pelletized to 13 mm φ × 1 mm under the condition of 4.5 MPa for 5 min. Gold electrodes were vapor–deposited with cross–sectional area of 28.3 mm^2 on both surfaces of the $PbSnF_4$ pellet using an ion coater (IC–50; Shimadzu Corp.).

The pellet was set in a cell assembly that was designed specially to measure the electrical conductivity, as shown in Fig. 2.4; the pellet was sandwiched and pressed between two Pt electrodes. The electrical conductivity was measured using ac impedance method (Frequency Response Detector Model 1025, Potentiostat / Galvanostat Model 273A; EG & G Instruments). This measurement was done for frequencies of 500 kHz and 1 Hz. Temperature variations of ac conductivities were recorded for temperatures of 286–473 K. The polarization current was recorded as a function of time and was recorded using a computerized data acquisition system. The ac conductivities depicted the Arrhenius behavior of $PbSnF_4$ using a temperature variation setup.

The ion transport number of the sample was estimated using Wagner's dc polarization method [33]. Before dc polarization measurement, the electrical conductivity of the sample in argon was measured. After heating to an appropriate temperature, voltage was applied and the leak current was measured using chronoamperometry (Potentiostat / Galvanostat Model 273A; EG & G Instruments) using the same setup. The steady volt–ampere characteristics of the specimen were also measured. Partial electron hole and electronic conductivities were obtained. Then, the electronic transport number was calculated.

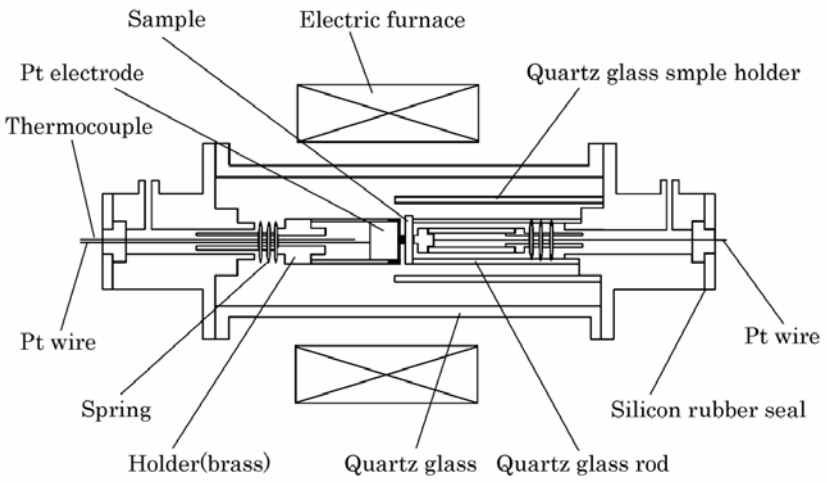

Fig. 2.4. Schematic illustration of the original designed cell.

2.2.3 Preparation of COF_2

Fig. 2.5 is an image of a CO_2 / F_2 electrochemical cell. It is expected that the electrochemical cell would be applied at a low temperature by our research.

A CO_2 / F_2 electrochemical cell was constructed using a reactive line and an original cell for electromotive force measurement. A $PbSnF_4$ disk was prepared for the electromotive force measurement. A sample of about 2.5 g was compacted into a pelleter. After vacuuming for 15 min, the sample was pelletized to 20 mm φ × 1.2 mm under 9.5 MPa for 5 min. The relative density of the pellet of the $PbSnF_4$ prepared here was about 0.87.

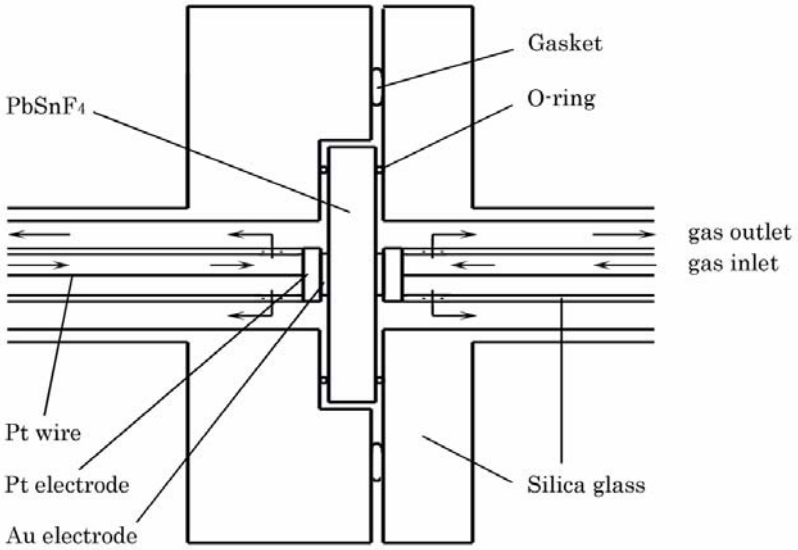

Fig. 2.5. Schematic diagram of the CO_2 / F_2 electrochemical cell.

The pellet was polished and a porous Au electrode was vapor–deposited onto the $PbSnF_4$ pellet surface. Fig. 2.5 shows that the pellet was set in a cell assembly designed specially to measure the electromotive force. In addition, the cell was connected to an original line, as shown in Fig. 2.6.

The CO_2 and F_2 in Ar, Argon balance, were put in the cell, respectively, in 0.1 MPa and the electromotive force was measured. That arrangement produced a closed circuit and the current was measured when the electromotive force was steady.

The CO_2 gas of the anode side was put in an IR cell after the current had been measured in the closed circuit for three hours at 373 K. The gaseous product at the anode was analyzed using FT–IR spectroscopy.

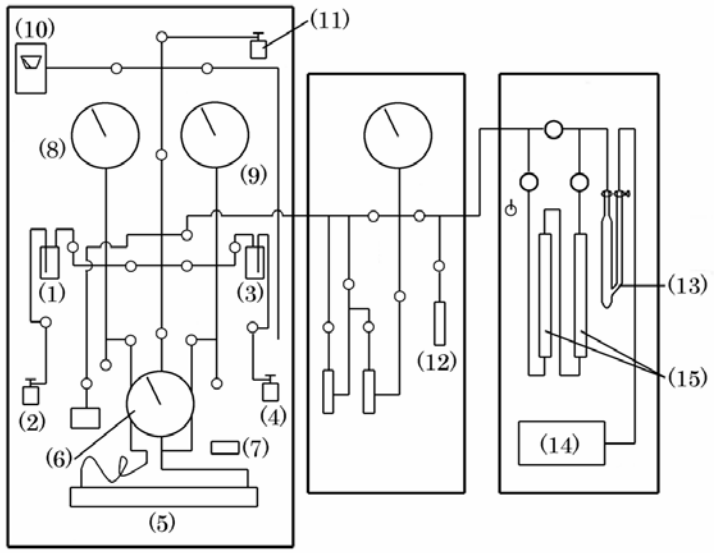

Fig. 2.6. Schematic diagram of original line for electromotive force measurement. (1) CO_2 gas storage, (2) CO_2 gas cylinder, (3) F_2 gas storage, (4) F_2 gas cylinder, (5) cell for electromotive force, (6) F_2 gas pressure gauge, (7) F_2 gas pressure digital gauge, (8) CO_2 gas pressure gauge, (9) F_2 gas pressure gauge, (10) PIRANI gauge, (11) Ar gas cylinder, (12) gas sampler, (13) trap (liquid N_2), (14) vacuum pump (oil rotary), and (15) activated alumina.

2.3 Results and discussion

2.3.1 Preparation of $PbSnF_4$

A synthesis on the MF_2–SnF_2 systems in both aqueous and molten states was carried out by Donaldson and Senior [7]. There are two known main routes to prepare $PbSnF_4$ from solution and by direct reaction at high temperature [7–12].

White sediment was prepared by mixing a $Pb(NO_3)_2$ aqueous solution and SnF_2

solution. The dropping speed was 10 or 500 $mm^3\ s^{-1}$. The hold time after mixing two solutions was 0–24 h. The (0 0 ℓ) peak of tetragonal $PbSnF_4$ became larger with increasing hold time after mixing. It was suitable to prepare tetragonal $PbSnF_4$ at dropping speed 500 $mm^3\ s^{-1}$ further than dropping speed 10 $mm^3\ s^{-1}$. Fig. 2.7 shows the XRD results of the synthesized sample at various temperatures at a dropping speed 500 $mm^3\ s^{-1}$. The Miller indices are shown in Fig. 2.7.

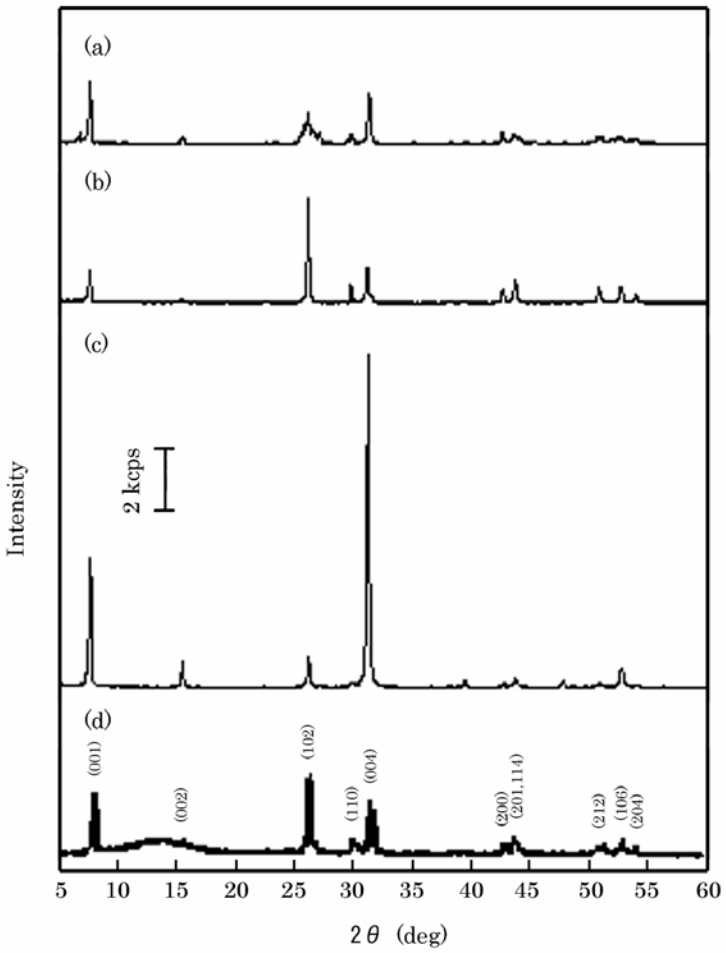

Fig. 2.7. XRD profiles of $PbSnF_4$ prepared at 273 K (a), 298 K (b) and 333 K (c), and reference (d).

Compared with Fig. 2.7(d) referred from the literature [11, 22, 34], a new peak was observed at $2\theta = 6.9°$; the (1 0 2) peak shape was broad at about 273 K. The (1 1 0) peak was almost lost, and the (0 0 ℓ) peaks had strengthened at about 333 K, and new small peaks were observed at 2θ = 39.5° and 47.8°. In this study, we obtained tetragonal $PbSnF_4$, as reported in Ref. [11], through preparation at room temperature.

Fig. 2.8 shows the profile of Rietveld refinement. The solid line in the profile was calculated using the RIETAN–2000 program [32]; the dotted line indicates data observed by XRD. The structure was determined in the tetragonal space group $P4/nmm$, with a_o = 0.4217 nm, c_o = 1.1427 nm; R_F was 7.09. This value was insufficiently small; some orthorhombic phase existed in the product.

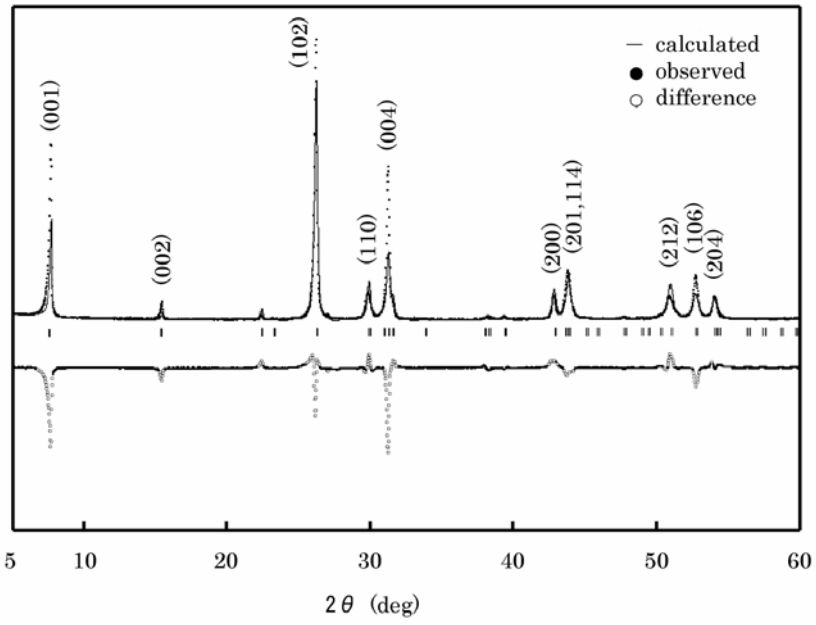

Fig. 2.8. Rietveld refinement profile of $PbSnF_4$. (－: calculated, ●: observed, ○: difference), R_F = 7.09, S = 9.1397.

A schematic illustration of the crystal lattice is shown in Fig. 2.9. Both Pb^{2+} and Sn^{2+} are ordered in the lattice. This ordering of Pb and Sn causes formation of vacancies of fluoride ion at the 4f and 8i site. Fluoride ions were transferred through these sites. Crystal parameters and interatomic distances are summarized in Tables 2.2 and 2.3. The theoretical density obtained from Rietveld refinement was 6.588 g cm^{-3} and the experimental density was 6.559 g cm^{-3}. The difference between the theoretical and experimental densities was 0.44%, which was considerably small.

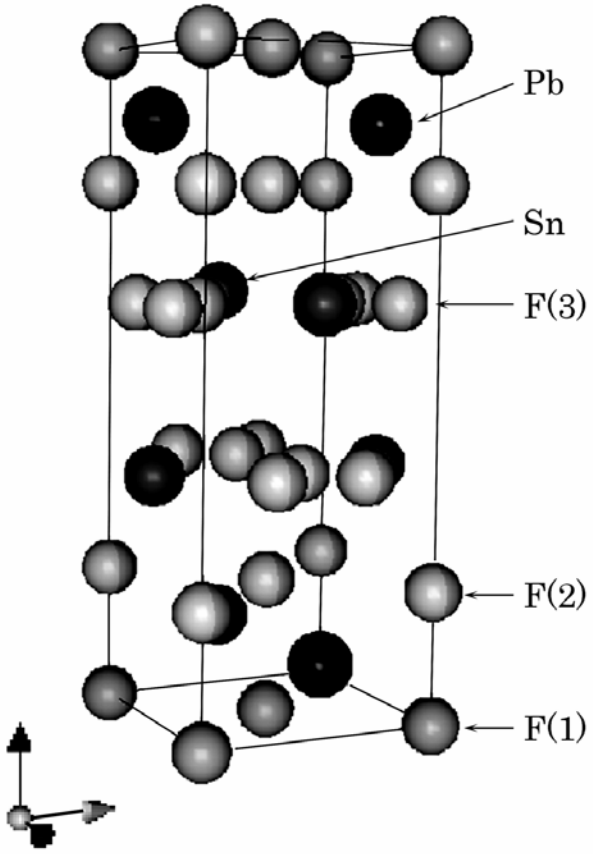

Fig. 2.9. Unit lattice of tetragonal $PbSnF_4$. a_o = 0.4217 nm, c_o = 1.1427 nm, Space group *P*4 / *nmm*.

On the other hand, the prepared sample was estimated, respectively, as $Pb_{1.2}SnF_{3.9}$, $PbSnF_{3.86-4.08}$ and $PbSnF_{3.8-4.12}$ using X–ray fluorescence spectroscopy (XFS), fluoride ion–selective electrode, and ion chromatography.

Table 2.2

Atomic parameter by Rietveld analysis of $PbSnF_4$

Atom	Site	x	y	z	Occupancy
Pb	2c	0	0.5	0.10995	1.0
Sn	2c	0	0.5	0.63036	1.0
F1	2a	0.5	0.5	0	1.0
F2	4f	0.5	0.5	0.2011	0.56
F3	8i	0	0.30901	0.37891	0.47

$V = 2.032 \times 10^{-28}$ m^3, Dx = 6.588×10^3 kg m^{-3}.

Table 2.3

Interatomic distance by Rietveld analysis of $PbSnF_4$

Bond	Length (nm)
Pb－F1	0.2454
Pb－F2	0.2351
Pb－F3	0.3177
Pb－Sn	0.4206
Sn－F1	0.4720
Sn－F2	0.2855
Sn－F3	0.2480
F1－F2	0.2297
F2－F3	0.2413
F3－F3	0.3324

2.3.2 Electrochemical properties

Fig. 2.10 shows a Cole–Cole plot of tetragonal $PbSnF_4$ in air. It shows that a semi–circular arc with a tail at the low–frequency range is assignable to electrode interface effects. This type of Cole–Cole plot is analyzed using Randles' equivalent circuit [27–29]. The center of the semi–circle is located below the real axis, which might show the inductance component arise from an experimental problem. At first, the Randles' circuit was inferred to be an equivalent circuit consisting of double–layer capacitance, the charge transfer resistance, and Warburg impedance. However, it seemed that the circuit was more complicated here.

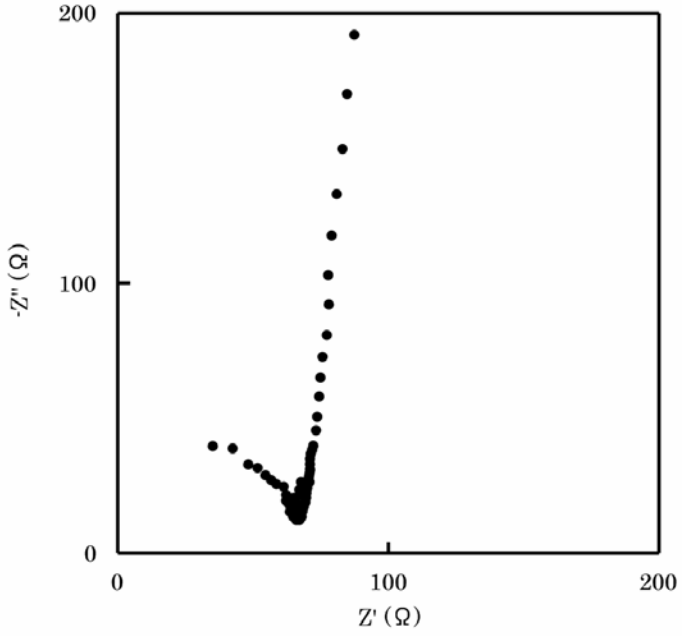

Fig. 2.10. Cole–Cole plot of tetragonal $PbSnF_4$ in air between 1 Hz and 500 kHz at 323 K. Sample thickness = 1 mm.

In this study, a linear part in the Cole–Cole plot was extrapolated to the high–frequency side and the value was regarded as resistance of the sample because factors were not calculable. The value of the extrapolated right crossing point of the impedance spectra to the real axis corresponding to dc resistance was about 65 Ω at 323 K. That is, dc conductivity was calculated as 0.54 Sm^{-1} at 323 K.

Fig. 2.11 shows Arrhenius plots of the electrical conductivity of tetragonal $PbSnF_4$ for temperatures of 286–473 K in various atmospheres.

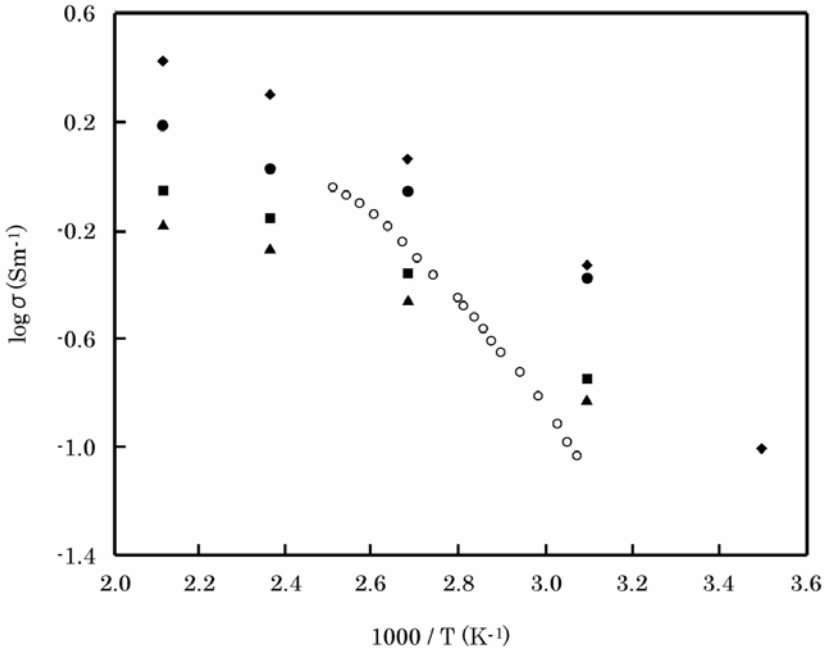

Fig. 2.11. Electrical conductivity of tetragonal $PbSnF_4$ upon cooling from 473 K to 286K. (a) In air (◆), (b) in vacuum (■), (c) in Ar (●) and in Ar flow (▲), and reference values (d) (○).

A value higher than the reference value in the literature [11, 13, 22] was obtained in air and Ar. Tetragonal $PbSnF_4$ exhibited the highest conductivity of 3.2 Sm^{-1} at 473 K in air. The electric conductivity rose with increasing temperature; the Arrhenius plot showed a gradual slope change around 373 K from the high–temperature range to the low–temperature range in good agreement with the literatures. The activation energies were estimated as 25.0 kJ mol^{-1} at 373–286 K and 12.4 kJ mol^{-1} at 473–373 K.

The phase transitions in $PbSnF_4$ were already reported around 355 K [13, 17, 22]. It has been reported that the change in the slope of Arrhenius plots of tetragonal $PbSnF_4$ are found around 355 K from the high–activation–energy region to the low–activation–energy region in the literatures [8, 17, 22, 35].

Tetragonal $PbSnF_4$ might transform to the other phase, which has lower conductivity. Observed disagreements with values obtained from the literature might result from the different tetragonal $PbSnF_4$ concentration in the sample.

The ionic transport number of mobile species was estimated using Wagner's polarization method [33]. Fig. 2.12 shows the chronoamperogram of $PbSnF_4$ at 373 K. The current observed at 474 K was not sufficiently stable to carry out measurements. It increased gradually with elapsed time. The current was not well measured at 323 K either, because the current is so small in this case. At 423 K, the currents used at the steady state were 1.95 and 21.0 nA for applied voltages of 0.1 and 0.5 V, respectively. For 373 K, the currents were 0.38 and 8.13 nA for 0.1 and 0.5 V of the applied voltages, respectively. Results of chronoamperometry at 423 and 373 K are summarized in Table 2.4. The total current i includes both ionic and electronic currents. The electrons and holes contribute to the electronic current. The electron transport number (τ_e) was obtained using the following equation:

$$I / [\exp(u) - 1] = RT[\sigma_h + \sigma_e \exp(-u)] / FL,\ u = EF / RT$$

Therein, I is the current density, F the Faraday constant, approximately 96,500 coulombs per equivalent, L the thickness of the sample, E the applied voltage, σ_h is the hole conductivity, and σ_e is the electron conductivity. The electronic current was carried the electrons mainly because $\sigma_h \ll \sigma_e$. The electronic conductivities ($\sigma_h + \sigma_e \fallingdotseq \sigma_e$) were much smaller than the electrical conductivities of 1.52 and 1.13 Sm^{-1} (423 and 373 K), respectively. Therefore, the ionic transport number was found to be approximately 1. The tetragonal $PbSnF_4$ seems to be a good fluoride ion conductor.

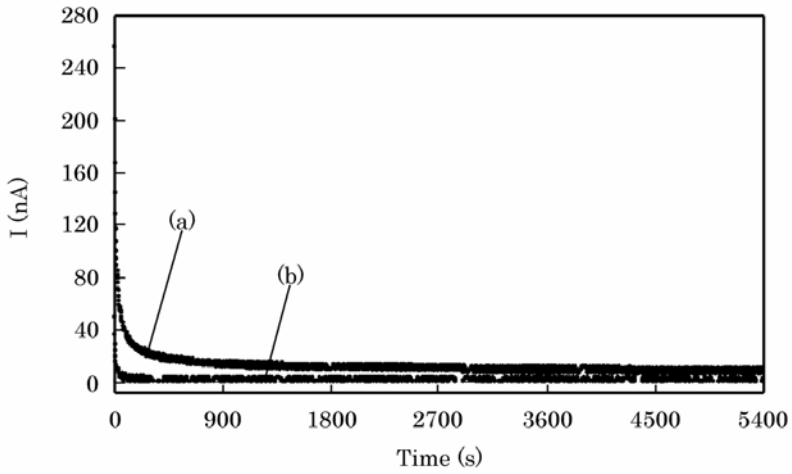

Fig. 2.12. Chronoamperometry for $PbSnF_4$ at 373 K. Applied p.d. = 0.5 V (a), 0.1 V (b). Sample thickness = 1 mm.

Table 2.4

Conductivities taken by electron and hole, σ_e and σ_h in $PbSnF_4$ at 423 and 373 K

Temperature (K)	Electron conductivity, σ_e (Sm^{-1})	Hole conductivity, σ_h (Sm^{-1})
423	4.4×10^{-5}	4.4×10^{-10}
373	9.5×10^{-6}	3.2×10^{-11}

2.3.3 Preparation of COF_2 in an electrochemical cell

We reported the reaction between CO_2 and F_2 to form COF_2 [4]. By that reaction, CO_2 is convertible to COF_2. The Gibbs free energy change of this reaction is calculated as –220 kJ mol^{-1} [5]. The theoretical electromotive force (emf) calculated from its Gibbs free energy is 1.14 V; that value is mostly equal to 1.23 V of the emf for the H_2 / O_2 fuel cell [6]:

$$CO_2 + F_2 \rightarrow COF_2 + 1/2\ O_2 + (-\Delta G)\ 220\ kJ\ mol^{-1}$$

A CO_2 / F_2 electrochemical cell was constructed with a tetragonal $PbSnF_4$ disk having Au electrodes.

The reactions at anodes and cathodes are written as follows:

Anode: $2\ F^- \rightarrow F_2 + 2\ e^-$,

$CO_2 + F_2 \rightarrow COF_2 + 1/2\ O_2$

Cathode: $F_2 + 2\ e^- \rightarrow 2\ F^-$

Therefore, $CO_2 + F_2 \rightarrow COF_2 + 1/2\ O_2$. As shown above, the tetragonal $PbSnF_4$ [7–21] is

known as a fluoride ion conductor having high electric conductivity at ambient temperature. The CO_2 / F_2 electrochemical cell was constructed using tetragonal $PbSnF_4$ with Au electrodes as the solid electrolyte; its performance was investigated using emf and impedance measurements.

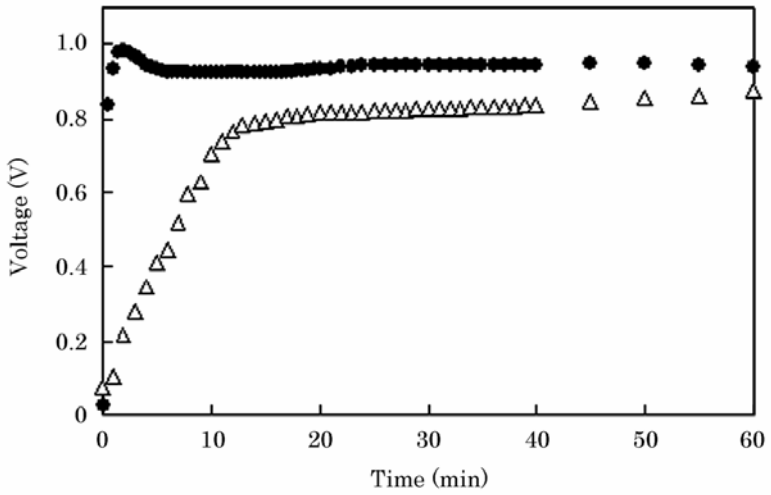

Fig. 2.13. The change in emf over time. Anode gas was 0.1 MPa CO_2 and cathode gas was χ MPa F_2 + (0.1 − χ) MPa Ar. (●: χ = 0.02, △: χ = 0.01).

Fig. 2.13 shows results of emf measurements under conditions of 0.1 MPa CO_2 / (0.02 MPa F_2 + 0.08 MPa Ar) and 0.1 MPa CO_2 / (0.01 MPa F_2 + 0.09 MPa Ar). The respective emf values were about 0.93 V and 0.86 V at 0.02 MPa F_2 and 0.01 MPa F_2 in Ar. The measured emf value was about 80% of the theoretical one of 1.14 V. The difference between the emf value for 10–20% F_2 in Ar was calculated as 0.009 V. Commonly, the chemical potential becomes lower by the interfacial resistance of the electrolyte and the electrode or the crossleak. Although some points require improvement, a CO_2 / F_2

electrochemical cell can probably be constructed sufficiently with $PbSnF_4$ as a solid electrolyte. However, the measured short circuit current density was 0.24 A m^{-2}, which was quite small.

Fig.2.14 shows Cole–Cole plot of tetragonal $PbSnF_4$ in the electrochemical cell. Fist, the impedance was measured under the condition of 0.1 MPa Ar / 0.1 MPa Ar at anode and cathode sides. And then, Ar gas was eliminated from the cathode side and substituted by F_2 gas. The charge transfer resistance and double layer capacitance changed by contacting F_2 gases to the electrolyte.

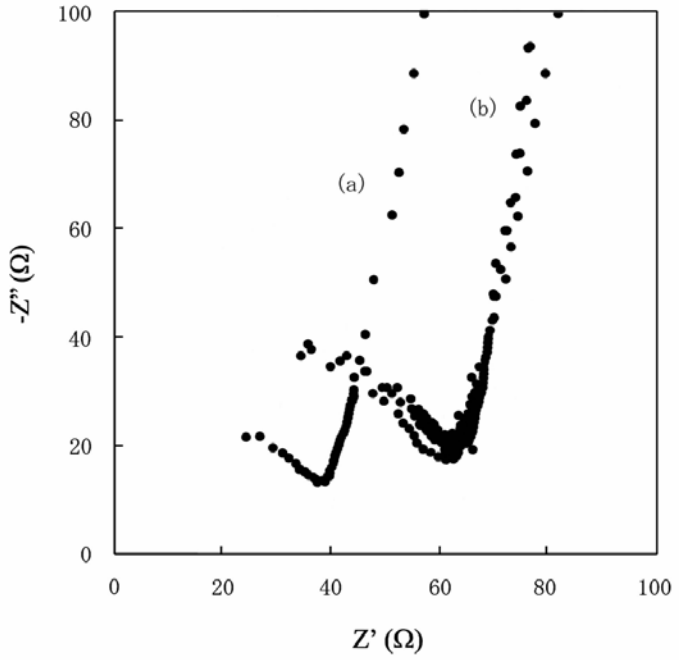

Fig. 2.14. Cole–Cole plot of tetragonal $PbSnF_4$ between 1 Hz and 500 kHz at 373 K. (a) Anode and cathode gases were Ar, (b) anode gas was Ar, cathode gas was F_2 gas.

It is important to mention here that the resistance, capacitance and impedance changed and became large by the effect of F_2 gas during the measurement. Apparently, the current value did not increase according to the effects of the morphological stability of electrode against F_2 gas. The electrolyte and the electrode interface might be very sensitive to F_2 gas, and the charge transfer process and mass transfer process might be affected by the exposure time of the sample under the F_2 environment.

The absorption peaks of fluorocarbon compound did not appear in the FT–IR spectra in which 1200–1300 cm^{-1} and around 1930 cm^{-1} corresponded to C–F and CF=O bonds, respectively. The current density was so small that the reaction between CO_2 and F_2 could not take place sufficiently and no fluorocarbon compound was detectable after 3 h discharge using FT–IR.

References and Notes

[1] I. Omae, Nisankatannso to Tikyukankyou, Tyukousinnsho (1999) pp.23–142. http://cdiac.esd.ornl.gov/trens/emis/em_cont.htm.

[2] Y. Matsumoto, M. Obata, and J. Hombo, J. Phys. Chem. 98 (1994) 2950–2951.

[3] W. M. Sears and S. R. Morrison, J. Phys. Chem. 89 (1985) 3295–3298.

[4] Y. Hasegawa, R. Otani, S. Yonezawa, M. Takashima, J. Fluorine Chem. 128 (2007) 17–28.

[5] J. C. Amphlett, J. R. Dacey, G. O. Pritchard, J. Phys. Chem. 75 (1971) 3024–3026.

[6] W. M. Latimer, The Oxidation States of the Elements and their Potentials in Aqueous Solutions (Prentice Hall, New York, 1952).

[7] D. J. Donaldson, B. J. Senior, J. Chem. Soc. (A) 1821–1825 (1967).

[8] J. M. Reau, C. Lucat, J. Portior, P. Hagenmuller, L. Cot, S. Vilminot, Mat. Res. Bull. 13 (1978) 877–882.

[9] J. Pannetier, G. Denes, J. Lucas, Mat. Res. Bull. 14 (1979) 627–631.

[10] G. Perez, S. Vimont, W. Granier, L. Cot, C. Lucat, J. M. Reau, J. Portior, P. Hagenmuller, Mat. Res. Bull. 15 (1980) 587–593.

[11] G. Denes, M. C. Madamda, A. Muntasar, A. Peroutka, K. Tam, and Z. Zhu, Nato, Sci. Ser. 25–38 (1999).

[12] G. Denes, J. Solid State Chem. 77 (1988) 54–59.

[13] G. Denes, T. Birchall, M. Sayer, M. F. Bell, Solid State Ionics 13 (1988) 213–219.

[14] Y. Ito, T. Mukuyama, H. Funatomi, S. Yoshikado, T. Tanaka, Solid State Ionics 67 (1994) 301–305.

[15] R. Kanno, K. Ohno, H. Izumi, T. Kamiyama, H. Asamo, F. Izumi,Y. Solid State Ionics 70–71 (1994) 253–258.

[16] G. Denes, Y. H. Yu, T. Tyliszczak, A. P. Hitchcock, J. Solid State Chem. 91 (1991) 1–15.

[17] M. M. Ahmad, K. Yamada, T. Okuda, J. Phys.: Condens. Matter 14 (2002) 7233–7244.

[18] S. Suda, T. Eguchi, J. Kuwano, Key Engineering Materials 181–182 (2000) 203–206.

[19] A. Wakagi, J. Kuwano, Y. Saito, J. Mater. Chem. 41 (1994) 973–975.

[20] T. Eguti, S. Suda,T. Hijii, S. Koga, J. Kuwano, Y. Saito, Key Engineering Materials 181–182 (2000) 199–202.

[21] A. Wakagi, J. Kuwano, M. Kato, H. Hanamoto, Solid State Ionics 70–71 (1994) 601–605.

[22] G. Denes, G. Milova, M. C. Madamda, M. Perfiliev, Solid State Ionics 86–88 (1996) 77–82.

[23] M. J. Sienko, R. A. Plane, Chemistry: Principles and Properties (McGraw-Hill, Inc. 1966).

[24] J. B. Goodenough, Pure & Appl. Chem. 67 (1995) 931–938.

[25] A. J. Bard and L. R. Faulkner, Electrochemical Methods; Wiley & Sons: New York, 2001; Chapters 3, 5, 7, 10, 13

[26] W. Schmickler, Interfacial Electrochemistry; Oxford University Press: Oxford, 1996.

[27] J. E. B. Randles, Discuss. Faraday Soc. 1 (1947) 11–19.

[28] J. E. B. Randles, Trans. Faraday Soc. 44 (1948) 327–338.

[29] J. E. B. Randles, Trans. Faraday Soc. 52 (1956) 1573–1581.

[30] R. Parsons, Chem. Rev. 90 (1990) 813–826.

[31] Y. Li, J. Gao, G. Yu, Y. Cao, A. J. Heeger, Chem. Phys. Lett. 287 (1998) 83–88.

[32] F. Izumi and T. Ikeda, Mater. Sci. Forum 321–324 (2000) 198–203.

[33] J. B. Wagner and J. C. Wagner, J. Chem. Phys. 26 (1957) 1597–1601.

[34] Joint Committee for Powder Diffraction Standards (JCPDS), International Centre For Diffraction Data.

[35] R. Kanno, S. Nakamura, K. Ohno, Y. Kawamoto, Mat. Res. Bull. 26 (1991) 1111–1117.

Chapter 3

Conclusion and future work

3.1 Conclusion

From the results presented, it is confirmed that the reaction between CO_2 and F_2 for preparation of COF_2 takes place spontaneously. A CO_2 / F_2 electrochemical cell produced enough open circuit voltage about 0.9 V, while it could produce quite small amount of electric power.

3.1.1 Chapter 1

By the reaction between CO_2 and F_2, COF_2 was obtained at high yield in conditions of 473 K during 50 h in a direct reaction. The by–products were CF_3OF and CF_4. All of NaF, CsF and EuF_3 were tested as catalysts. Results showed that CsF can play a role as the catalyst. The COF_2 formation rates in the presence of CsF were five times larger than that without catalyst. Using CsF, the yields of COF_2 and CF_3OF become higher than that in the direct reaction for temperatures of 373–473 K. In addition, $CF_2(OF)_2$ was produced at 303 K and its yield decreased with increasing temperature; CF_3OOCF_3 was detected more at 473 K. Yields of COF_2 and CF_3OF become higher than that in the

direct reaction at temperatures of 373–473 K. The slightly lower amount of CF_4 less than 0.1% was produced in this case. The CsF affected the reaction pathways. For the reaction without CsF, the $F^{\cdot}$ formation plays an important role in the products' composition. Considering that COF_2 is converted into CF_3OF, the best yield of COF_2 was 11.1% under the reaction conditions of CO_2 / F_2 = 76 kPa / 76 kPa, with temperature of 498 K and 72 h reaction time in the direct reaction. The reaction mechanism in the presence of CsF can be explained using the formation of possible reaction intermediates $[CF_2(OF)O^{\delta-}Cs^{\delta+}F]$ and $[CF_3O^{\delta-}Cs^{\delta+}F]$ at each temperature. The best yield of COF_2 was 6.5% under the reaction conditions of CO_2 / F_2 = 76 kPa / 76 kPa with 473 K reaction temperature and 50 h reaction time.

3.1.2 Chapter 2

Tetragonal $PbSnF_4$, which had higher electrical conductivity than orthorhombic $PbSnF_4$, was prepared by adding $Pb(NO_3)_2$ aqueous solution to SnF_2 aqueous solution at dropping speed of 500 $mm^3\ s^{-1}$ at room temperature. The tetragonal $PbSnF_4$ exhibited conductivity of 3.2 Sm^{-1} at 473 K in air.

A CO_2 / F_2 electrochemical cell was constructed using tetragonal $PbSnF_4$ with Au electrodes as the solid electrolyte. The electromotive force was about 0.9 V at room temperature under conditions of 0.1 MPa CO_2 / (0.01 MPa F_2 + 0.09 MPa Ar). The short circuit current density was measured as 0.24 A m^{-2}.

The content of the fluorocarbon compound as the product was so low that it could not be detected.

3.2 Future work

None of the CO_2 / F_2 fuel cell device systems has been reported to date. We have proposed a new energy cycle with CO_2 fixing process, and reported the performance of CO_2 / F_2 electrochemical cell. There has been a tremendous interest because of the potential for the energy cycle including the reaction between CO_2 and F_2 as one method for CO_2 fixation. The prospect of using a CO_2 / F_2 electrochemical cell as an application for CO_2 fixation would be very appealing and has a deep impact on our society.

Our study has led to a significant progress in understanding a CO_2 / F_2 fuel cell and its reactions. However, its performance was very low. It indicates that the CO_2 / F_2 fuel cell had many difficulties. The poor chemical stability of the materials limited the all performances. The fundamental study to design the materials which are anti–corrossive by F_2 might contribute to solve it.

List of publications

1 Journal papers:

[1] “Reaction between carbon dioxide and elementary fluorine,” Yasuo Hasegawa, Reiko Otani, Susumu Yonezawa, Masayuki Takashima, J. Fluorine Chem., 128, 17–28 (2007).

[2] “Preparation of COF_2 using CO_2 and F_2 in the electrochemical cell with $PbSF_4$ as a solid electrolyte,” Yasuo Hasegawa, Akitomo Nagasaka, Jae–Ho Kim, Susumu Yonezawa, Masayuki Takashima, J. Fluorine Chem., 128, 958–964 (2007).

2 Conference papers:

[1] “Reaction between carbon dioxide and elementary fluorine,” Satoshi Ueda, Yasuo Hasegawa, Susumu Yonezawa, Masayuki Takashima, International Chemical Congress of Pacific Basin Societies, Honolulu, Hawaii, December, 2000, Book of Abstracts, P. 1487.

[2] “The reaction between carbon dioxide and elementary fluorine in the presence of various fluorides,” Reiko Otani, Yasuo Hasegawa, Susumu Yonezawa, Masayuki Takashima, Fusso Kagaku Touronkai Koen Youshishu, Vol. 25th, 109–111 (2001).

[3] “Preparation of $PbSF_4$ as a solid electrolyte,” Akitomo Nagasaka, Hidezi Fukaya, Shigeyuki Kimura, Yasuo Hasegawa, Susumu Yonezawa, Masayuki Takashima, The International Conference on Fluorine Chemistry, Kyoto, Japan, May, 2004, Book of Abstracts, P. 8.

[4] 二酸化炭素とフッ素ガスの反応, Hiroyasu Otsuka, Masaru Miyamoto, Yasuo Hasegawa, Susumu Yonezawa, Masayuki Takashima, 第 21 回フッ素化学討論会講演予稿集, P–09, 112 (1997).

[5] 二酸化炭素とフッ素ガスの反応, Hiroyasu Otsuka, Masaru Miyamoto, Yasuo Hasegawa, Susumu Yonezawa, Masayuki Takashima, 日本化学会北陸地区講演会予稿集, D–12, 68 (1997).

[6] 二酸化炭素とフッ素ガスの反応, Masaru Miyamoto, Satoshi Ueda, Yasuo Hasegawa, Susumu Yonezawa, Masayuki Takashima, 日本化学会北陸地区講演会予稿集, D–12, 68 (1999).

[7] フッ素－二酸化炭素の直接反応に関する触媒の検討, Reiko Otani, Takashi Yagi, Satoshi Ueda, Yasuo Hasegawa, Susumu Yonezawa, Masayuki Takashima, H12 年度日本化学会北陸地区講演会予稿集, D–13 (2000).

[8] フッ素－二酸化炭素の直接反応機構の解析, Reiko Otani, Yasuo Hasegawa, Susumu Yonezawa, Masayuki Takashima, H13 年度日本化学会北陸地区講演会予稿集, D–10 (2001).

Articles of other works

1 Journal papers:

[1] 水中におけるミッシュメタルの発火危険性, Tadashi Uno, Yasuo Hasegawa, Takashi Yamamuro, 安全工学, 27, 157–161 (1988).

[2] ＭｍＮｉＡｌ系水素吸蔵合金のアルカリ水溶液中での表面変化と電気化学挙動, Masayuki Takashima, Yuiti Matsumura, Yasuo Hasegawa, Gentarou Kanou, Keiiti Hasegawa, Masahiko Oshitani, Yuji Matsumaru, 電気化学 60, 231–238 (1992).

[3] ミッシュメタルの物性に関する研究, Yasuo Hasegawa, 警察庁法科学研修所研究報告集, 139–156 (1992).

2 Conference papers:

[1] ＤＩ／ＭＳによるポリマーの定性, Yasuo Hasegawa, Tadashi Uno, 鑑識科学研究発表会講演集（1990）.

[2] ＭｍＮｉＡｌ系水素吸蔵合金の充放電反応およぼすコバルトの影響（１）, Masayuki Takashima, Yuiti Matsumura, Yasuo Hasegawa, Gentarou Kanou, 電気化学協会北陸支部 30 周年記念大会, B19 (1991).

[3] ＭｍＮｉＡｌ系水素吸蔵合金の充放電反応およぼすコバルトの影響（２）, Masayuki Takashima, Yuiti Matsumura, Yasuo Hasegawa, Gentarou Kanou, 電気化学秋季大会, 2F27 (1991).

[4] 基本的な高分子熱分解物の昇温ＥＩ／ＣＩＭＳ法による検討, Yasuo Hasegawa, 第 28 回北陸質量分析談話会 (1993).

[5] 昇温ＥＩ／ＣＩＭＳ法，ＴＧ／ＭＳ法による基本的な高分子化合物のマススペクトルの比較, Yasuo Hasegawa, 日本鑑識科学技術学会第 1 回学術集会講演要旨集, C–10, 50 (1995).

[6] “Preparation and properties of neodymium–europium oxide,” Masayuki Takashima, Susumu Yonezawa, Yasuo Hasegawa, A. Unishi, International Chemical Congress of Pacific Basin Societies, Honolulu, Hawaii, December, 1995, Book of Abstracts, P. 1666.

[7] Kinetic Method によるメタンフェタミンのプロトン親和力測定の試み, Shigeki Matsumura, Tetuya Tsukahara, Yasuo Hasegawa, Hideyuki Takezawa, Kimio Isa, 日本鑑識科学技術学会第 6 回学術集会講演要旨集, C–5, 50 (2000).

3 Books:

[1] 薬物事犯対策のための調査研究報告（パラオ共和国）, Kimiyoshi Nakano, Satoru Onishi, Yoshiaki Maedomari, Yasuo Hasegawa, Shinji Kabayashi, （財）全国防犯協会連合会, 1999.